GOTHIC Aerosol Source Depletion Studies

Spent Fuel and Waste Disposition

Prepared for
U.S. Department of Energy
Spent Fuel and Waste Science and Technology

Pacific Northwest National Laboratory
Mark S. Lanza, Mike Leimon,
Mohamed Elsawi, Andrew Casella

April 16, 2021

M3SF-21PN010207042
PNNL-31176

SUMMARY

Pacific Northwest National Laboratory has continued work to develop an aerosol-laden flow modeling capability with the Generation of Thermal Hydraulic Information in Containment (GOTHIC™) computer code to perform simulations for thermal hydraulic conditions and aerosol transport and deposition in spent fuel casks.

This report describes our recent work to expand our model that was originally developed in 2019 to allow for thermal characterization, carrier gas velocity characterization, and tracking of particulate behavior throughout the entire canister volume. The expanded model capability was achieved through conversion of radioactive decay heat source in all fuel tubes within the model from heaters to thermal conductors in GOTHIC as well as remeshing the internal volume of the canister. In GOTHIC, heaters are a tool that are used to specify heat sources within specified regions of the model, while thermal conductors allow for GOTHIC to couple the fuel pin and He gas energy equations to calculate temperature of fuel and He gas with decay heat source and heat transfer at the fuel clad-He gas interface. These improvements allowed for temperatures, carrier gas velocities, and particulate concentrations to be determined throughout the entire model space, which was not possible in the previous version of the model. Several characteristics of the GOTHIC code were elucidated by the current study and were documented for consideration in how the code is used for modeling aerosol transport and deposition in spent fuel casks moving forward. For instance, treatment of particle size distributions, initial spatial distributions of particles, mesh gradients, and minimum volume concentrations were identified as important issues for consideration. Ultimately, the current version of the code is capable of tracking temperatures, flow rates, and particle behavior throughout the canister internal volume. This report presents predicted depletion times and preferred deposition patterns within the canister. Additionally, this report documents code performance and insights for further model development and use for future comparisons to analyses using other codes and for predicting system behavior in experiments being performed and planned by our collaborators.

This page is intentionally left blank.

ACKNOWLEDGEMENTS

The authors would like to thank Richard Daniel for the technical review of this document.

This report was developed with significant contributions, expert input, and guidance from Sam Durbin at Sandia National Laboratories and from the GOTHIC developers Tom George and Jeff Lane at Zachry Nuclear Engineering.

This page is intentionally left blank.

CONTENTS

This page is intentionally left blank

.

LIST OF FIGURES

LIST OF TABLES

ACRONYMS

AED	aerodynamic equivalent diameter
GSD	geometric standard deviation
SMD	Sauter mean diameter
BC	boundary condition
CFL	Courant-Friedrichs-Lewy condition
GOTHIC	Generation of Thermal Hydraulic Information in Containments
MELCOR	Methods for Estimation of Leakages and Consequences of Releases
ORNL	Oak Ridge National Laboratory
PNNL	Pacific Northwest National Laboratory
PWR	pressurized water reactor
SCC	stress corrosion crack
SNF	spent nuclear fuel
SNL	Sandia National Laboratories
STP	standard temperature and pressure
TSC	transportable storage container

This page is intentionally left blank.

GOTHIC AEROSOL SOURCE DEPLETION STUDIES

1. INTRODUCTION

As long-term dry storage of spent nuclear fuel generated at US nuclear power plants remains the currently exercised option for the back end of the nuclear fuel cycle, research efforts remain in place to ensure that these dry storage facilities remain effective in maintaining the integrity of the spent fuel over extended time periods. One key aspect of these efforts is to identify and characterize any potential storage system degradation mechanisms that may threaten storage container integrity so that appropriate mitigation efforts can be enacted. One such degradation mechanism that is currently identified as a prominent concern is stress corrosion cracking (SCC) leading to a through-wall breach in a dry storage container. The occurrence of a through-wall breach creates a pathway for release of components of the container internal environment to the external environment with the potential unintended release of radioactive material outside of its containment and possible contamination of the facility and workers where the fuel cask is stored. This possible release pathway leads to the need to understand the release consequences of this release pathway and mitigate the risk of breach occurrence and release exposure. Specifically, there is a need to characterize 1) the expected composition of the internal environment of the storage container and 2) the transport of this environment through the through-wall breach.

Initially defining the internal environment of a dry storage container is straight forward; however, predicting that environment through time and several potential physical scenarios quickly becomes very complex. For instance, at the time of closure of the container, the total container volume, fuel rod decay heat, and quantity of back fill gas can be used to determine cask temperatures, pressures, and convection currents over time. However, if through any mechanism, the spent fuel cladding barrier is breached, and gases or particulates are allowed to pass from within spent fuel rods to the dry cask interior, then mixed gas and aerosol transport within the cask can have significant impacts on those analyses. Additionally, spallation of materials such as corrosion products on the outside of the spent fuel rods can contribute to an aerosol source term within the container. In addition to phenomena that may occur while the dry storage container is static (such as cladding failure or spallation), mechanical upset conditions will lead to additional gas and particulate dispersion within the container; particulate suspension, transport, and deposition (depletion) generate even more interest.

Upon the formation of a through-wall breach in the storage container, different phenomena are of primary interest depending upon the internal conditions of the container.

- If the internal condition of the storage container remains pristine and a through-wall breach were to form, then the blow-down of the internal environment until pressure equilibrium is reached can be estimated with the size and shape of the through-wall crack introducing the largest uncertainty to the analysis. The issues of greatest concern in such a scenario is impact of the loss of backfill gas on the thermal condition within the container and any potential introduction of oxygen or moisture from the outside environment into the container.
- If any fission gases or volatile components were present within the fill gas at the time of the through-wall breach formation, then their release to the external environment is of concern. If suspended particulates are present, then the problem becomes more complicated and potentially more impactful as 1) the greatest level of radioactivity is present in solid form within the container and could be transported out of the container as particulates and 2) particulates can deposit within the through-wall breach leading to plugging.

The complexity and potential impact of scenarios involving particle suspension and SCC-induced through-wall cracks has led to the substantial efforts of characterization of such scenarios by the current program. These efforts include large-scale experiments as well as multiple modeling endeavors. As many length scales are of interest in aerosol phenomena, many different modeling techniques complement

one another in attempting to address this problem. Oak Ridge is currently developing a phenomenological model in Python while Sandia is using a combination of MELCOR and FLUENT to characterize this system of interest. This report is focused on the use of the engineering-scale GOTHIC code to supplement current experimental and cooperative modeling efforts to address the particular issue of suspended particulate deposition behavior within a dry spent fuel storage container.

This page is intentionally left blank.

2. BACKGROUND

The potential release of particulates from a dry used fuel storage canister after the formation of a through-wall crack has been recognized as a topic of concern for some time. Efforts have been made to develop models capable of characterizing such release scenarios and have been reported in (Casella, Loyalka, & Hanson, 2014) (Mitrakos, et al., 2008). In 2018, the current program made the decision to begin using the Generation of Thermal Hydraulic Information in Containment (GOTHIC) computer code (GOTHIC, 2018) to expand modeling characterization capabilities for these systems. This effort resulted in the development of two separate models; one characterizing the internal conditions of a dry storage container, and one characterizing flow through a micro-scale flow pathway representing a through-wall breach (Lanza, Casella, Elsawi, Carstens, & Springfels, 2019). Subsequently, substantial effort was put into advancing the latter model in order to complement simultaneous microchannel flow experiments performed at Sandia National Laboratories (SNL) (Lanza, Azuma, Carstens, & Casella, 2020) (Durbin, Lindgren, & Pulido, 2018). This report presents current advances in the dry cask container model representing the characterization of conditions within the dry used fuel container. This effort is being performed in parallel with efforts at Oak Ridge National Laboratory (ORNL) to refine their phenomenological model and at SNL to update MELCOR.

This page is intentionally left blank.

3. OBJECTIVE

Models describing aerosol behavior are complex. Modeling of aerosol dynamics not only account for heat and mass transfer in the suspending phase (where flow is most likely turbulent or subjected to natural convection) but also include terms to account for interactions between the particles themselves (including particle agglomeration) and the bounding surfaces of the container (particle deposition) and phoretic phenomena (gravity, electrophoresis, etc.).

Additionally, when the aerosol systems of interest are confined to small geometries or particulate populations, efforts become even more complicated as average behavior and statistics associated with large populations become less applicable. The problem of diffuse particulate dispersions within a dry storage container involving restricted channel flow paths and eventually a restrictive breach flow path falls into the very complicated category. In an attempt to address this system of interest with all of its complexities, the current research effort involving PNNL, ORNL, and SNL has focused on comparing different modeling approaches in order to elucidate parameters and spaces of high impact to ensure that models are truly accurate and indicative of the system. To this end, a set of simplified systems with prescribed initial conditions and modeling parameters was agreed upon for each of the modeling teams to tackle toward the end of cross comparison and collaborative advancement.

PNNL has updated the internal cask model developed and reported on in 2019 (Lanza, Casella, Elsawi, Carstens, & Springfels, 2019) so that it is capable of tracking particulate transport and deposition throughout the entirety of the internal volume of the storage container. The objectives of this report are to:

1. describe model updates in the current work,
2. describe the simplified systems defined for cross-code comparisons and discuss the results of simulations in GOTHIC, and
3. discuss the aspects of the GOTHIC code that became impactful (both positive and negative impacts are discussed in the results and conclusion) to this effort.

A discussion of the modeling approach in GOTHIC as evaluated with parameter sensitivity analyses is also included in the current report to highlight what the GOTHIC code is doing and to ensure that future efforts will be aware of 1) the key issues impacting model fidelity and 2) the model adjustments needed to generate accurate, useful results.

During the study we identified limitations stemming from the simplifications made for baseline model code-to-code comparisons. While convenient for comparison purposes these simplifications neglect the subtleties that characterize aerosols. Most significant is the aerosol size distribution which is ignored with monodisperse representations and precludes some aerosol phenomenon such as gravitational settling which arises due to the settling rate of particles of different size, affecting the time dependent deposition of the aerosol. This study provided a useful means of evaluating the limitations inherent in monodisperse models and afforded a deeper understanding of the aerosol modeling capability and operation of GOTHIC.

4. GOTHIC MODELS

GOTHIC (GOTHIC, 2018) is an integrated finite volume, general-purpose thermal-hydraulics software package for design, licensing, safety, and operating analysis of nuclear power plant containment, confinement buildings, and system components. GOTHIC includes the basic equations of continuity, momentum, and energy and also has a feature to allow users/developers to add or modify equations for special calculations. We describe the basic capabilities of GOTHIC for aerosol mechanics and compressible flow modeling in our previous works (Lanza et al. 2019, Lanza et al. 2020). The current work supplements that description, allowing for a deeper understanding of the GOTHIC results which incorporate all of the noted effects simultaneously.

5. THERMAL HYDRAULIC CASK MODEL

The authors have previously developed a dry cask storage system model to simulate long term decay heat removal performance and the cask internal thermal-hydraulics (Lanza et al. 2019). That model served as the base for current work that implements multiple improvements to the base model; these improvements are discussed in Section 5.1.

The GOTHIC model was developed based on the MAGNASTOR spent fuel dry storage system (NAC International, 2011), shown in Figure 1. The model includes discretized fluid volumes that represent volumes within the concrete cask (CC) and transportable storage canister (TSC). The spent fuel basket internal to the TSC is modeled as 37 vertical fuel tubes connected hydraulically to common plena at the bottom and top of the TSC. The lower and upper plena are connected by the volume between the fuel basket and TSC shell, referred to here as the bypass volume. Each fuel tube (channel) is axially discretized (along the Z-axis). The lower and upper plena and bypass region are discretized in the X, Y, and Z axes. The space between the TSC and CC is modeled as 3 volumes: CC lower plenum, CC, and CC upper plenum. The CC plena are modeled as lumped volumes and the CC is an axially discretized volume. Axial discretization in the CC matches that in the TSC volumes.

The model includes the thermal mass and surface of all components in the storage system shown in Figure 1 as well as PWR spent fuel assemblies for a fully loaded configuration of the TSC. Thermal conductors for all components and fuel assemblies connect to fluid volumes to establish thermal communication between volumes.

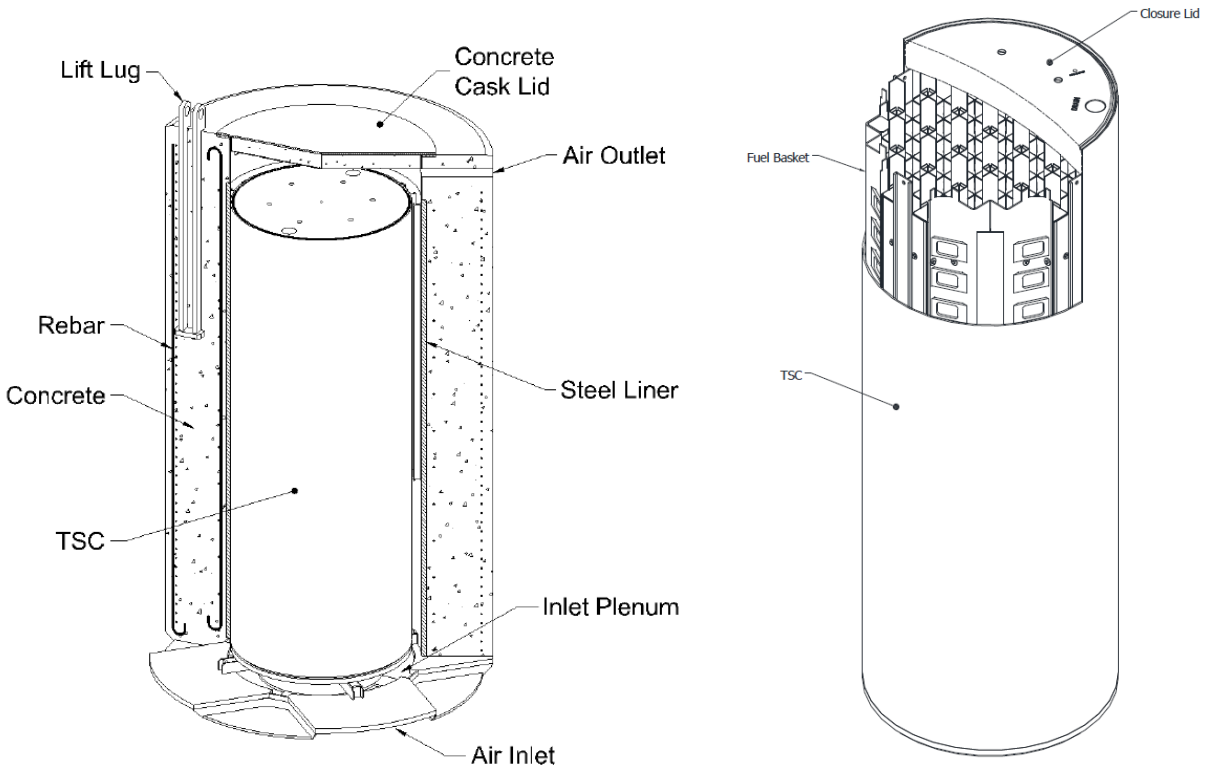

Figure 1. MAGNASTOR spent fuel dry storage system (left) and Transportable Storage Canister (TSC) (right).

A high-level schematic of the dry cask storage system GOTHIC model is shown in Figure 2. The model consists primarily of the components listed below.

1. Volumes 1s-37s, indicated by numbered yellow rectangles in Figure 2-a, are the 37 fuel tubes within the TSC basket. Each fuel tube is represented as a 1D volume axially subdivided (meshed) into 18 cells.
2. Volumes 38s-40s, indicated by numbered yellow rectangles in Figure 2-a, are 3D volumes that represent the TSC lower plenum, bypass, and upper plenum, respectively.
3. Volumes 41s-43s, indicated by numbered yellow rectangles in Figure 2-a, represent the concrete cask modeled as 3 volumes: lower plenum, annular space between cask shell and TSC shell, and cask upper plenum. respectively. The lower and upper plenums are 0D “lumped volumes”. The concrete cask annular volume is represented as a 1D volume subdivided axially.
4. Flow paths (FP) 1-80, indicated by green labeled lines in Figure 2-a, represent hydraulic connections between volumes and boundary conditions.
5. Pressure (P) and flow (F) boundary conditions (BC) 1P, 2F, 3F and 4F are indicated with numbered blue boxes in Figure 2-a.

   The concrete cask upstream BC(2F) represents the temperature and flow conditions entering from the external environment. The concrete cask downstream BC(1P) represents the ambient pressure condition. BC(3F) and BC(4F) are the aerosol injection temperature and mass flow rates.

6. Thermal conductors 1-131, indicated by red labeled lines in Figure 2-b, represent thermal structures and locations of heat transfer surfaces.

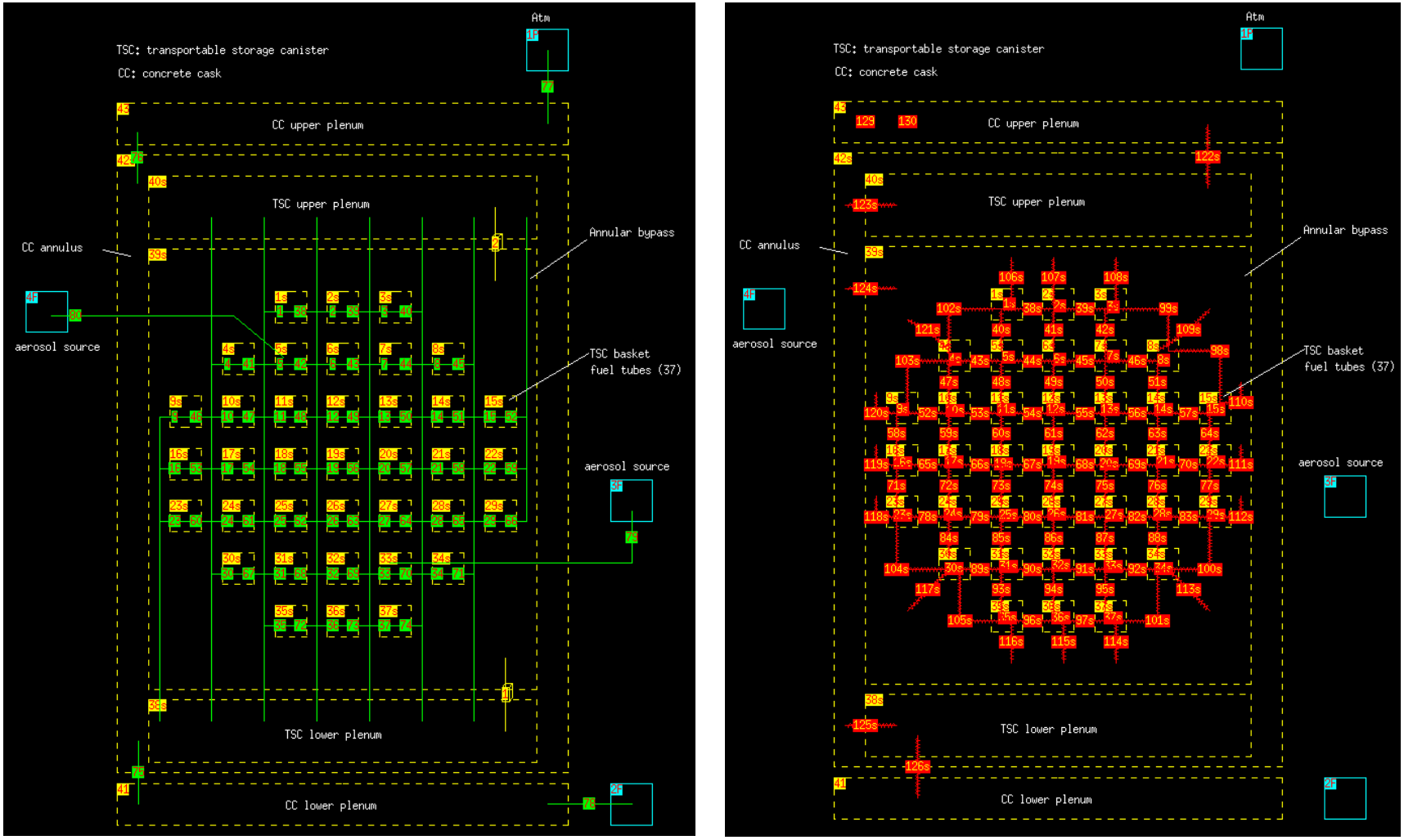

(a) **(b)**

Figure 2. Dry storage cask model schematic. Hydraulic "flow path" connections to volumes and BCs are shown in the left figure. Thermal conductors with connections to volumes are shown in the right figure.

5.1 Notable Changes from Previous Model

Refinements and improvements were made to the spent fuel dry cask storage system base model previously developed by Lanza et al (2019). Improvements included thermal structures representing the fuel assemblies in each fuel tube with internal heat generation for decay heat, replacing the heater components used before. The TSC lower and upper plenum, bypass, and concrete cask were upgraded to meshed volumes from the previous "lumped" 0D volumes. The 1D axial meshed volumes for 37 fuel tubes containing assemblies were refined for the axial dependence of fluid volume, flow area, hydraulic diameter, and laminar friction modeling. Boundary conditions for aerosol injection have been added to model aerosol transport within the TSC.

5.1.1 Control Volumes

5.1.1.1 Refined Nodalization

Several control volumes were converted from lumped control volumes over to being subdivided control volumes. These control volumes included the: TSC lower plenum, TSC upper plenum, and bypass control volumes. Since physically the free space in these control volumes was cylindrical in nature, this feature was modeled by the inclusion of one or more blockages. Since the blockages which provide shape to the model do so by removing free volume from the control volumes, the overall outer dimensions and free volume of the unblocked lumped volumes must first be increased (before subdividing the volume) so that the resultant total free volume of the subdivided volume is the same (as the original lumped volume) after the blockages are added.

Additionally, while the CC annulus control volume was already subdivided in the previous version, it was still being modeled in a relatively simplistic manner. Similar improvements were made to modeling of the cask annulus control as described in the previous paragraph.

5.1.1.1 TSC Internal Mesh

The TSC volumes compose the cask inner containment volume, which is the fluid volume accessible to aerosols in this model. TSC volumes include 37 fuel tubes containing assemblies, lower and upper plena, and the bypass volume (volume between TSC shell and fuel basket). Improvements were made to the mesh in these volumes to simulate local fluid flow and temperature conditions. An overview of the composite mesh is shown in Figure 3. The mesh shown at left in Figure 3 is composed of the separate GOTHIC subdivided volumes for the fuel tubes (37), upper and lower plena, and bypass volumes. A porous media approach is used to represent the effective volume and hydraulic diameter of the volume surrounding the spent fuel assembly in each fuel tube. Figure 3 does not indicate the internal porosity or surface area of the cells. In GOTHIC, all volumes are created with regular rectangular ordered meshes and the cell volume and surface porosity parameters are adjusted to affect shape of the internal domain. The mesh shown at right in Figure 3 shows the TSC lower plenum mesh with a circular blockage that blocks grey cells (porosity=0.0), resulting in a cylindrical shaped volume representing the lower plenum.

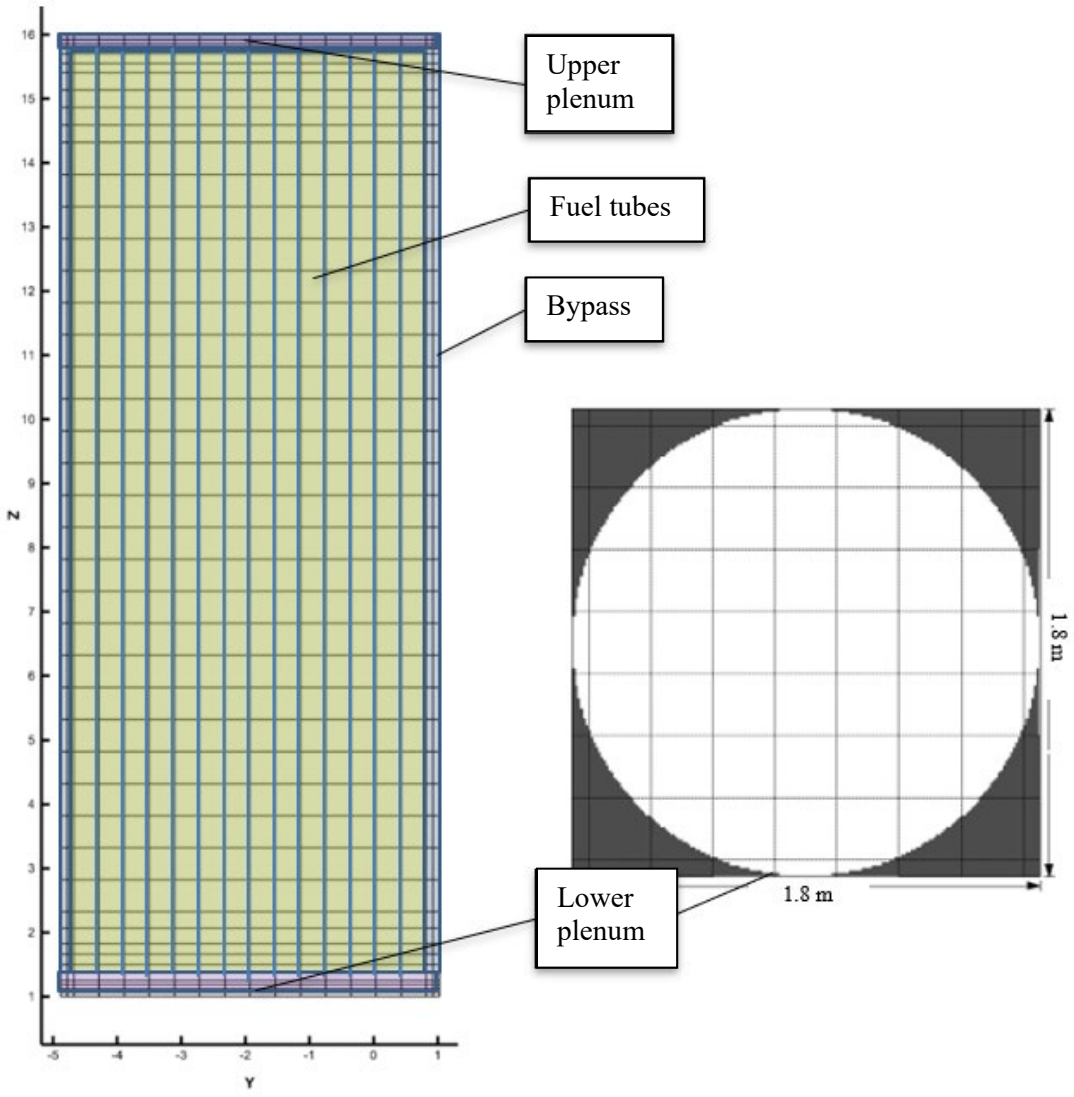

Figure 3. TSC internal fluid volume mesh Y-Z perspective (left) and X-Y perspective (right) with cylindrical blockage. Dimensions on mesh in the left figure are in feet.

The lower plenum control volume utilizes only a single blockage to model the characteristics of this volume. More specifically, this blockage is an exterior domain blockage type of cylindrical geometric form. This blockage is clearly visible within Figure 4: it is the shaded region around the periphery.

The lower plenum control volume was nodalized such that there are: nine (sets of) cells along the X axis, nine (sets of) cells along the Y axis, and two (sets of) cells along the Z axis. This nodalization is displayed here in Figure 4.

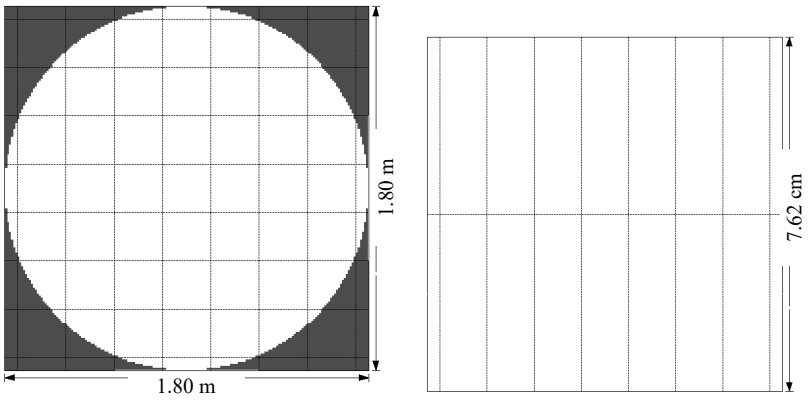

Figure 4. Lower plenum Y-X nodalization (left) and Z-X nodalization (right)

Along the Y-X plane the central set of 7x7 cells were sized so that they align with the sizing and placement of the individual dry cask assembly tubes. The final two bounding (outer) cells (along both the X and Y axis) were included to capture the volume which extends out to very limit of the free volume within the cylindrical geometry.

As for the Z axis (also visible in Figure 4), two vertical (sets of) cells were utilized to allow for flow circulation effects within the subdivided volume. This nodalization along the Z axis may seem minimal, however, it was selected to reduce simulation slowdown effects associated with the Courant-Friedrichs-Lewy (CFL) limit.

The upper plenum control volume was nodalized such that there are: nine (sets of) cells along the X axis, nine (sets of) cells along the Y axis, and two (sets of) cells along the Z axis. This nodalization is displayed here in Figure 5.

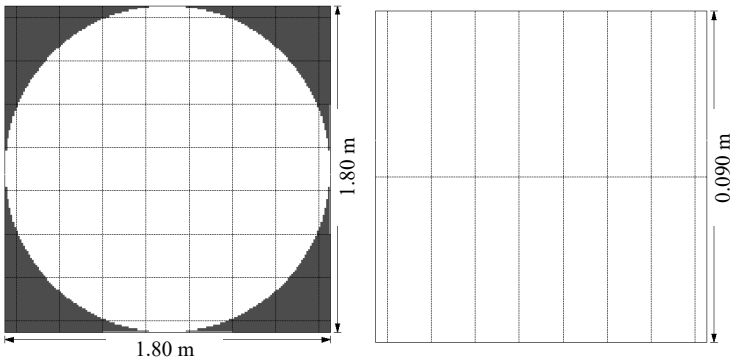

Figure 5. Upper plenum Y-X nodalization (left) and Z-X nodalization (right)

Along the Y-X plane the central set of 7x7 cells were sized so that they align with the sizing and placement of the individual dry cask assembly tubes. The final two bounding (outer) cells (along both the X and Y axis) were included to capture the volume which extends out to very limit of the free volume within the cylindrical geometry.

As for the Z axis (also visible in Figure 5), two vertical (sets of) cells were utilized to allow for flow circulation effects within the subdivided volume. This nodalization along the Z axis may seem minimal, however, it was selected to reduce simulation slowdown effects associated with the CFL limit.

While in theory, the free volume within this control volume (after being subdivided) should be roughly the same as it was when it was a lumped volume. The reality is that, the improved detail in modeling this physical space with a subdivided volume and blockages resulted in a roughly 37% reduction of free volume versus the value used for the lumped volume.

The bypass control volume was nodalized such that there are: nine (sets of) cells along the X axis, nine (sets of) cells along the Y axis, and 18 (sets of) cells along the Z axis. This nodalization is displayed here in Figure 6.

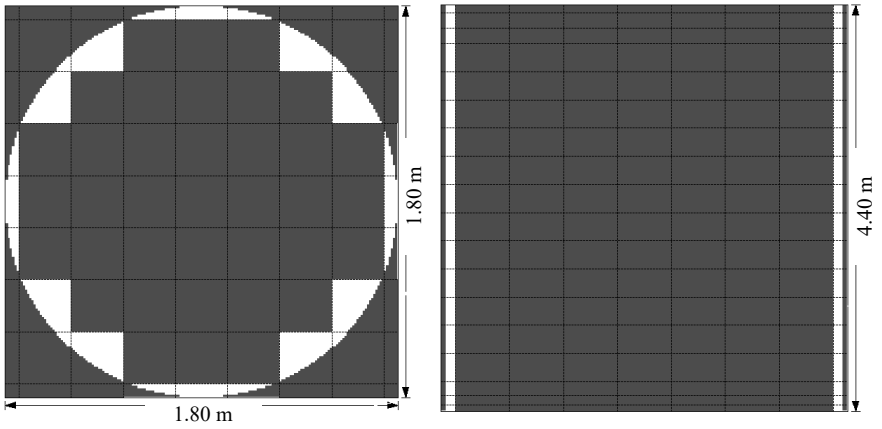

Figure 6. Bypass volume Y-X nodalization (left) and Z-X nodalization (right)

Along the Y-X plane the central set of 7x7 cells were sized so that they align with the sizing and placement of the individual dry cask assembly tubes. The final two bounding (outer) cells (along both the X and Y axis) were included to capture the volume which extends out to very limit of the free volume within the cylindrical geometry.

As for the Z axis (also visible in Figure 6), these cells were included and sized so that they align with the sizing and placement of Z axis cells within the various dry cask assembly tubes. The primary rationale for this design choice was for improving the modeling of thermal conductors. More specifically, this nodalization allows for more accurate calculation of thermal conduction between the various axial cells of the assembly tubes located in the periphery and the adjacent vapor space cells within the bypass volume.

The bypass control volume utilizes a total of 19 blockages to model the characteristics of this volume. While the physical aspects of this volume could have instead been modeled more easily by using a total of four blockages (three for the central assemblies and one for the TSC shell) a more detailed approach was instead taken. More specifically, all the outer assemblies (along the periphery of the cask) were modeled as separate blockages. The benefit of this modeling decision is that it enables the thermal conductors which transfer heat between the outer assemblies and the bypass volume to be spanned over the exposed area of these individual assembly blockages, therefore providing an accurate representation of the actual physical scenario. Finally, two more blockages were required to block out the rest of the volume occupied by the inner assemblies.

Given the rather complex configuration of the blockages within this subdivided volume, a more detailed visualization is provided within Figure 7. Do note that the blockage numbering used in this figure is for illustrative purposes only and doesn't necessarily correspond to the ordered list of blockages within the GOTHIC model. First there is the cylindrical blockage which bounds the internal volume of the TSC shell (this blockage is not numbered within Figure 7 but, it shown as the shaded region around the periphery). Next the outer assembly blockages are shown as blue regions and are labeled with numbers from 1 to 16. Finally, the inner assembly blockages are shown as red and gold regions within the figure and are labeled with numbers 17 and 18, respectively.

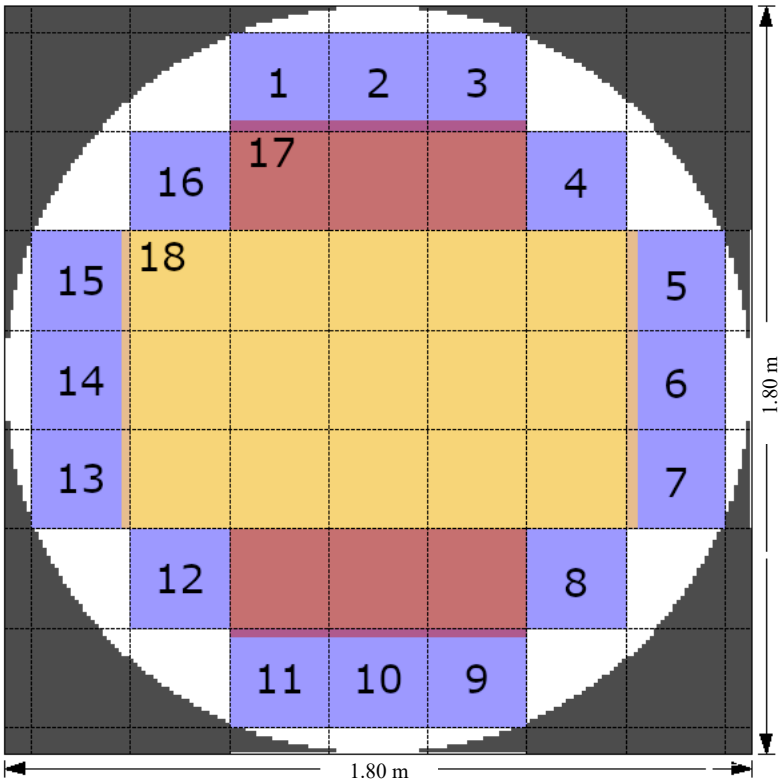

Figure 7. Bypass volume assembly blockages

5.1.1.2 Cask Annulus

While the cask annular space control volume was formerly a subdivided control volume, it was not a particularly detailed subdivided volume. Formerly, the 1D subdivided volume was modeled as a set of ten 1.5 ft vertical cells (shown in Figure 8). To go along with the upgrades to the bypass control volume, the nodalization of this subdivided volume was also improved. The updated nodalization for this control volume was selected and sized so that it aligns with the sizing and placement of Z axis cells within the bypass control volume. There are however, two more Z axis cells within the cask annulus volume than there are in the bypass control volume. These two additional cells correspond to the cask annular spaces which surround the upper and lower plenum regions.

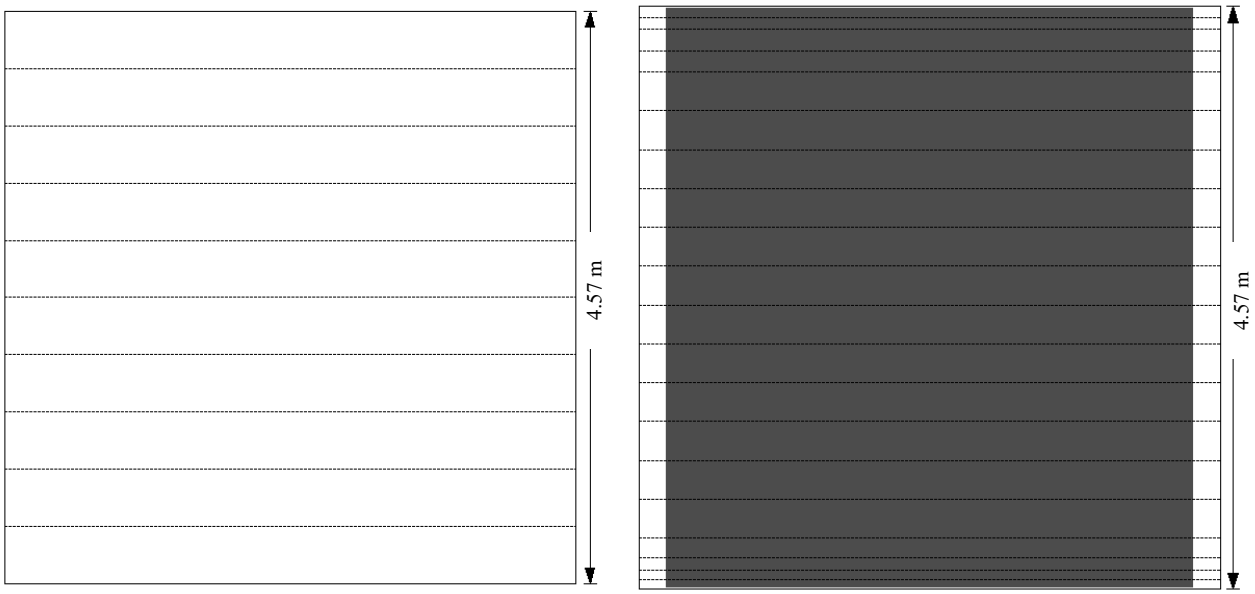

Figure 8. Cask annular space volume old Z-X nodalization (left) and new Z-X nodalization (right).

Another simplification that was present in the previous model was that blockages were not being used to carve out the actual void space from a volume of a bounding size. The outer dimensions of the cask annular space control volume were resized so that blockages could then be used to provide an accurate physical representation of the volume. While in theory, the free volume within this control volume (after being revised) should be roughly the same as it was before. The reality is that, the improved detail in modeling this physical space with a subdivided volume and blockages resulted in a roughly 37% reduction of free volume versus the value used for the original representation.

More specifically, the updated cask annular space control volume was nodalized such that there are: 20 (sets of) cells along the Z axis. This nodalization is displayed here in Figure 9.Figure 8

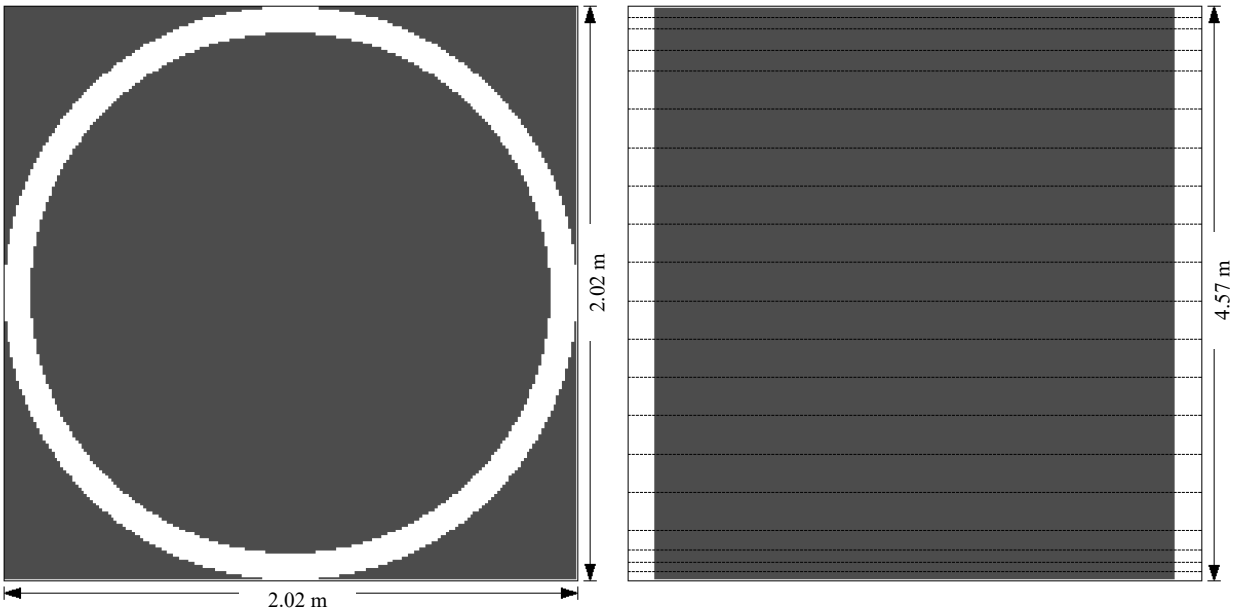

Figure 9. Cask annular volume Y-X nodalization (left) and Z-X nodalization (right).

The cask annular space control volume utilizes a total of four blockages to model the characteristics of this volume. First, the cask shell was modeled using a blockage that is an exterior domain blockage type of cylindrical geometric form. This blockage is clearly visible within Figure 9, it is the shaded region around the periphery. Next a set of three blockages were used to model the space occupied by the TSC. These three blockages which represent the TSC are all cylindrical in nature and differ only in blockage height and Z axis positioning. Essentially, the TSC lower plenum blockage only blocks the region which is within the bottom cell of the cask annular space control volume. Similarly, the TSC upper plenum blockage only blocks the region which is within the top cell of the cask annular space control volume. Finally, the TSC shell blockage occupies the central region for all the other cells within the cask annular space control volume. One of these three TSC blockages is also visible within Figure 9, it is the central shaded region.

The primary reason behind selecting this blockage configuration, has to do with improving heat transfer within the model. First separating the TSC shell into three separate blockages enabled usage of GOTHIC's capability to span the ends of a thermal conductor to the exposed surface of a blockage. It was essential that three separate blockages be used for the TSC shell, as one spanned thermal conductor was used to model heat transfer between the TSC upper plenum and the cask annular space, another used to model the heat transfer between the TSC lower plenum and the cask annular space, and finally another thermal conductor modeled heat transfer between the TSC bypass volume and the cask annular space. Using three blockages for these three spanned thermal conductors allowed heat transfer to be correctly mapped between adjacent Z axis cells within cask annular space volume and the other three control volumes.

5.1.2 Thermal Conductors

5.1.2.1 Fuel Thermal Conductors

Within the previous version of the dry cask storage system GOTHIC model, fuel assembly decay heat for the hot channel (i.e., fuel tube containing the peak power assembly) was introduced with a thermal conductor with internal heat generation and an axial power shape. Decay heat in the other 36 fuel tubes was introduced to the system with a heater component in each of the basket fuel tubes. The new model utilizes instead a spanned thermal conductor in every fuel tube. The total decay heat power for the initial cask loading configuration is 26.4 kW (25 Btu/s). Figure 10 shows the assembly power in each fuel tube. The axial power shape applied to each fuel assembly is shown in Figure 11.

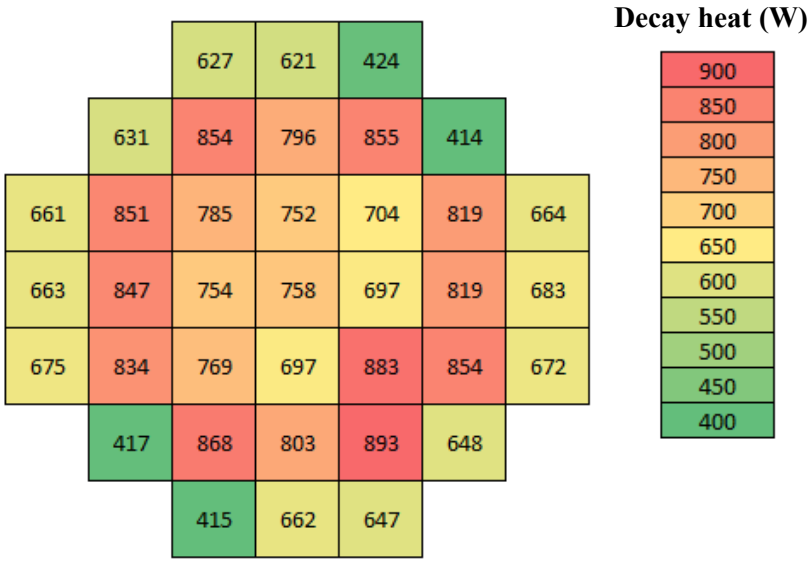

Figure 10. Assembly decay heat power (W) for the initial cask loading configuration.

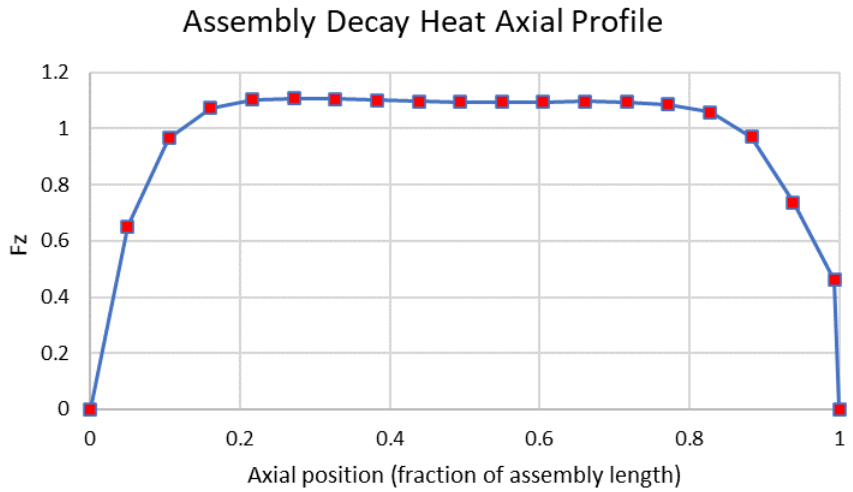

Figure 11. Assembly decay heat axial profile. Fz is equal to nodal power normalized to assembly average nodal power.

5.1.2.2 Respanning Thermal Conductors

In transitioning from lumped control volumes to subdivided control volumes, some thermal conductors had to be handled differently than before to achieve an equivalent effect. This section documents changes of this nature at a somewhat high level.

5.1.2.3 TSC Lower and Upper Plena

The TSC lower plenum control volume has a total of two external thermal conductors connected to it. The first of these thermal conductors is between the TSC lower plenum control volume and the cask annulus control volume. More specifically, one side of this thermal conductor is spanned over the TSC shell blockage within the TSC lower plenum control volume, while the other side of this thermal conductor is spanned to the TSC lower plenum blockage within the cask annulus control volume.

The second external thermal conductor connecting to the TSC lower plenum is the one which connects it to the concrete cask lower plenum. Within the TSC lower plenum control volume, this thermal conductor is spanned along the floor (-Z axis). The other end of this thermal conductor is within a lumped control volume.

The configuration for the TSC upper plenum is essentially the same as it is for the TSC lower plenum except that the connections are between the TSC upper plenum and other volumes. Additionally, for the external thermal conductor connecting to the TSC upper plenum to the concrete cask upper plenum, this thermal conductor is spanned along the ceiling (+Z axis) of the TSC upper plenum control volume.

5.1.2.4 Bypass

The bypass control volume has a total of 18 external thermal conductors connected to it. The first of these thermal conductors is between the bypass control volume and the cask annulus control volume. In more detail, one side of this thermal conductor is spanned over the TSC shell blockage within the bypass control volume, while the other side of this thermal conductor is spanned to the TSC shell blockage within the cask annulus control volume.

The second thermal conductor models the connection between the concrete cask standoffs and the TSC shell. To be consistent with the modeling from the previous version, it is simply spanned over the entire free volume of the bypass control volume. Finally, there are 16 external thermal conductors which connect the 16 outer assembly baskets to the bypass control volume. One side of each of these thermal conductors is spanned along one of the walls (+X, -X, +Y, or -Y axis) of each of the outer assembly tube control volumes, while the other side of these thermal conductors were spanned over the surface of the corresponding outer assembly blockage (shown in Figure 7) within the bypass control volume.

5.1.2.4.1 Cask Annulus

The cask annulus control volume has a total of four thermal conductors connected to it. The first of these thermal conductors is between the cask annulus control volume and the TSC lower plenum control volume. More specifically, one side of this thermal conductor is spanned to the TSC lower plenum blockage within the cask annulus control volume, while the other side of this thermal conductor is spanned over the TSC shell blockage within the TSC lower plenum control volume.

The second of these thermal conductors is between the cask annulus control volume and the TSC upper plenum control volume. In more detail, one side of this thermal conductor is spanned to the TSC upper plenum blockage within the cask annulus control volume, while the other side of this thermal conductor is spanned over the TSC shell blockage within the TSC upper plenum control volume. The third of these thermal conductors is between the cask annulus control volume and the bypass control volume. In more detail, one side of this thermal conductor is spanned to the TSC shell blockage within the cask annulus control volume, while the other side of this thermal conductor is spanned over the TSC shell blockage within the bypass control volume.

Finally, the last thermal conductor represents the connection between the cask annulus and the concrete overpack wall. This final thermal conductor is an internal thermal conductor which is spanned over all cells within the cask annulus control volume.

5.1.3 Hydraulic Junctions

5.1.3.1 New 3D Connectors

In transitioning from lumped control volumes in places over to subdivided control volumes, some flow paths had to be switched out for a 3D connector to achieve an equivalent effect. A total of two new 3D connectors were added to this model. The first of these 3D connectors is the one used to connect the lower plenum control volume to the bypass control volume. This 3D connector connects the topmost X-Y plane of cells within the lower plenum control volume to the bottom X-Y plane of cells within the bypass control volume. The second of these 3D connectors is the one used to connect the bypass control volume to the upper plenum control volume. This 3D connector connects the topmost X-Y plane of cells within the bypass control volume to the bottom X-Y plane of cells within the upper plenum control volume.

5.1.3.2 Reconnecting Flow paths

In transitioning from lumped control volumes in places over to subdivided control volumes, some flow paths had to have one of their ends reconnected to a specific cell face of a now subdivided volume to achieve an equivalent effect. These flow paths fell into one of two categories, flow paths which connected the lower plenum control volume to an assembly tube control volume or flow paths which connect assembly tube control volumes to the upper plenum control volume.

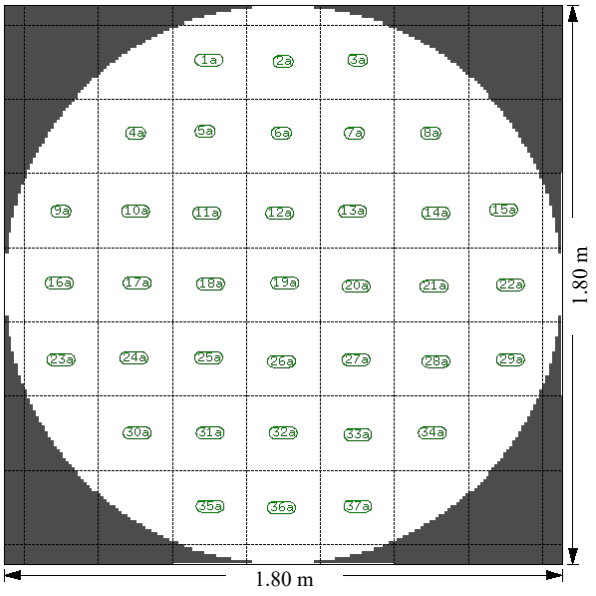

Figure 12. Lower plenum volume with fuel tube flowpath connections.

All the newly connected flow path endings which connect the lower plenum control volume to the various fuel tube control volumes are visible in Figure 12. Note that all these end connections are within the topmost X-Y plane of cells within the lower plenum control volume. The other end connections for these flow paths, located at the bottom of the fuel tube volumes, remained unchanged.

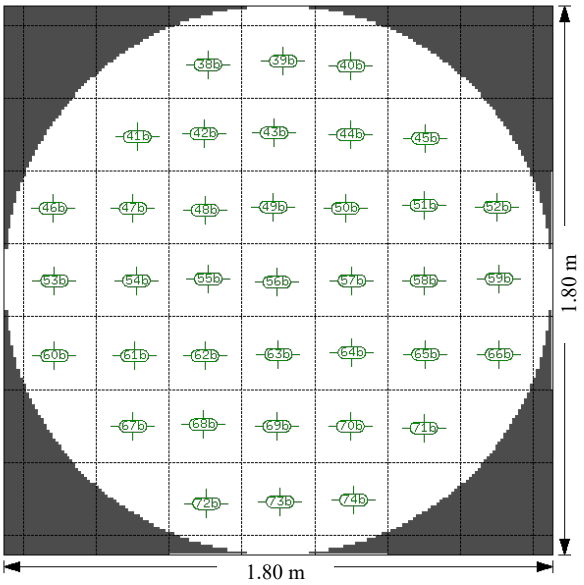

Figure 13. Upper plenum fuel tube flowpath connections

All the newly connected flow path endings which connect the various fuel tube control volumes to the upper plenum control volume are visible in Figure 13. Note that all these end connections are within the bottom X-Y plane of cells within the upper plenum control volume. The other end connections for these flow paths, located at the top of the fuel tube volumes, remained unchanged.

5.1.4 Boundary Conditions

Boundary conditions on the cask volume represent air flow from the environment that enters the concrete cask through vents at the bottom of the cask. Air flows upward between the TSC and concrete cask, cooling the TSC, and then exits the concrete cask through vents at the top of the cask. A boundary condition supplies 0.68 kg/s (1.5 lbm/s) air at 24.4 °C (76 °F) to the bottom vent and a simple atmospheric pressure boundary condition provides an exit for air at the top of the cask.

The other boundary condition is used to inject aerosol into one or two fuel tube channels representing the hypothetical release of aerosols from a ruptured fuel rod.

5.1.5 Friction Resistance in Fuel Tube-Assembly

Todreas and Kazimi (2012) present laminar and turbulent pressurized water reactor (PWR) fuel assembly pressure drop correlations that provide a good approximation to the assembly average fluid drag. The laminar correlation has the same form as the standard laminar friction model in GOTHIC. The standard model fRe=64 was modified to fRe=94.3. Both the fuel assembly correlation implemented with GOTHIC control variables and the standard model provided good results.

6. AEROSOL MODELING

6.1 Aerosol Size Distribution

GOTHIC drop field models, combined with liquid solid component models, provide the basis for dry aerosol modeling. By default, GOTHIC treats liquid drops as one or more separate fields governed by aerosol interactions, entrainment, and thermodynamics. A dry aerosol is modeled in GOTHIC by specifying the solid component volume fraction inside of drops to 1.0. Setting the solid component volume fraction to 1.0 removes all moisture from the drop composition and excludes the influence of phase change on the aerosol characteristics. Specifying the solid component fraction is necessary for dry aerosol modeling, otherwise the drop composition and field characteristics are subject to phase change. A drop with 100% solid volume fraction is considered a particle in this work although GOTHIC nomenclature consistently uses the term drop to refer to wet and dry drop fields. The term drop is used in this work to refer to the drop field models in GOTHIC.

Any number of drop fields can be used to track and simulate drop behavior in a GOTHIC model. It is assumed that the drops for a given field in a given cell have a log normal size distribution and that within each cell, each field is characterized by an average drop diameter and the geometric standard deviation (GSD) (Lane, et al., 2018). If drops are from a single source (e.g. spray system) a single drop field is typically adequate to model the drop behavior. Complex drop/particulate fields can be modeled using two or more fields.

For a log-normal distribution, approximately ninety-five percent of the drops will fall with the range

$$\sigma_g{}^{-2}\mathrm{CMD} < d < \sigma_g{}^{2}\mathrm{CMD}$$

where d is the drop diameter, CMD is the count median diameter, and σ_g is the GSD. This is the approximated Sauter Mean diameter (SMD) for the field.

The SMD of an aerosol field is equivalent to the diameter of average surface area for the field, which is also equivalent to the diameter of average projected area for the field. Drop momentum and heat transfer relationships in GOTHIC use the SMD.

The SMD d_{smd} by definition is

$$d_{smd} = \frac{6V_d}{A_d} \tag{1}$$

where V_d is the total volume of drops and A_d is the total surface area of drops. GOTHIC represents the drop fields dynamically with conservation balance equations for the surface area density and drop count density that together define the drop field. From the surface density a SMD is calculated which can have a log-normal distribution (i.e., GSD > 1.0). Dividing Eq. 1 by the fluid volume, the drop volume fraction and surface area density are related to the Sauter mean diameter as:

$$d_{smd} = \frac{6\alpha_d}{A_d{}'''} \tag{2}$$

Here α_d is the drop volume fraction and $A_d{}'''$ is the surface area density. The total drop surface area density is related to the drop count density $N_d{}'''$ and average surface area A_d as:

$$A_d{}''' = N_d{}'''A_d = \pi N_d{}'''d_{smd}{}^2 \tag{3}$$

Combining Eq. 2 and Eq. 3, the drop count density $N_d{}'''$ is

$$N_d{}''' = \frac{6\alpha_d}{\pi d_{smd}{}^3} \tag{4}$$

When drops are added to the system the newly created drops are added to the field whose nominal diameter is closest to the specified or calculated diameter for the new drops. GOTHIC tracks drop

concentrations that have a corresponding volume fraction larger than a specified minimum value. The default minimum volume fraction corresponds to 1 drop per cm^3 and depends on the nominal diameter as given by

$$\alpha_{min} = \left(\frac{\pi {d_{SMD}}^3}{6}\right) \times \left(\frac{1\, particle}{cm^3}\right) \tag{5}$$

where d_{SMD} is the nominal diameter in cm. This volume fraction allows tracking of drops to a concentration as low as 1 drop/cm^3. Eq. 5 is derived from Eq. 4 with N_d''' equal to 1 drop/cm^3.

The SMD resulting from a mix of two monodisperse fields is determined from the count density and SMD of each field. The count density of each field is equal to the ratio of volume fraction to drop size. The drop count density scales as 1/d^3; therefore, for an equal mix of two monodisperse sizes (bi-disperse), the resulting mixed diameter is

$$d_{ij} = \left(\frac{2}{\frac{1}{d_i^3}+\frac{1}{d_j^3}}\right)^{1/3} \tag{6}$$

which reveals that the resulting diameter d_{ij} will always be biased toward the smaller of the premixed diameters d_i and d_j. The mixed field SMD can generally be determined for any number of monodispersed fields with known volume fractions or concentrations. Eq. 6 is for the special case of two monodisperse fields of equal concentration as present in the bidisperse cases evaluated in this work.

As GOTHIC uses a log-normal distribution for drop sizes the Hatch-Choate conversion equations are valid and useful for converting CMD to the SMD (Heintzenberg, 1994).

$$d_{smd} = \mathrm{CMD} exp\left(\frac{5}{2}\left(\ln\sigma_g\right)^2\right) \tag{7}$$

For monodisperse aerosols, the geometric standard deviation (GSD) σ_g is unity and the conversion above simplifies to $d_{smd} = \mathrm{CMD}$.

6.2 Aerodynamic Equivalent Diameter

The aerodynamic equivalent diameter (AED) is the diameter of a unit density (water at standard temperature and pressure [STP]) sphere having the same settling terminal velocity (due to gravity) as the particle of interest of whatever shape and density. The relationship between particle diameter d_p and the AED (d_{AED}) is established from the Stokes settling velocity, which can be written as:

$$v_t = \frac{\rho_m {d_p}^2 g}{18\mu} = \frac{\rho_w {d_{AED}}^2 g}{18\mu} f_s \tag{8}$$

Here f_s is a dynamic shape factor, which for a spherical particle is equal to 1.0. ρ_w and ρ_m are the water and particle material density, respectively at STP. μ is the vapor dynamic viscosity and g is the gravitational acceleration. Simplifying Eq. 8, the particle diameter d_p for a given AED (d_{AED}) is calculated with the following equation.

$$d_p = d_{AED}\sqrt{\frac{\rho_w f_s}{\rho_m}} \tag{9}$$

All aerosol simulations performed in this work begin with an injection of a monodisperse field (GSD=1.0). For GSD = 1.0, the SMD d_{SMD} is equal to the CMD, taken to be the particle diameter, d_p for monodisperse fields in the current work.

6.3 Aerosol Concentration

This study considered nominal aerosol concentrations of 0.5, 1.0, and 10.0 mg/m^3 with a fixed particle density 10.97 g/cm^3 at standard temperature and pressure (i.e., T=298 K, P=101 kPa). The standard concentrations are adjusted to the cask internal temperature and pressure with the ideal gas equation. An average cask temperature was derived from calculations of the steady state thermal hydraulic solution for the initial loading decay heat identified in Section 5.1.2.

A scaling factor F_s is derived by holding mass constant

$$m = C_1 V_1 = C_2 V_2 \tag{10}$$

C_1 and V_1 are the STP concentration and volume, respectively that contain mass m. V_1 and V_2 depend on pressure and temperature. To determine the concentration of aerosol in cask internal conditions, mass is held constant and the change in volume is determined from the change in pressure and temperature from STP to conditions within the cask. Here, the development of F_s assumes that the gas is ideal.

$$PV = nRT \tag{11}$$

Concentration within the cask is

$$C_2 = \frac{V_1}{V_2} C_1 = \frac{T_1 P_2}{P_1 T_2} C_1 = F_s C_1 \tag{12}$$

T_1 and P_1 are 25 °C and P=101 kPa. The cask internal pressure for initial decay heat loading is P_1=701 kPa. T_2 is the cask average temperature for initial loading decay heat conditions. T_2=200 °C is the average of lower and upper plenum temperatures and T_2=210 °C is the average of lower plenum and peak temperature in the fuel tubes. Scaling factors for the average temperatures of 200 °C and 210 °C are 4.38 and 4.28, respectively. 4.38 was used to scale concentrations in Cases 1b and 2b and 4.28 was used in Case 3b

6.4 Aerosol Mechanics

The agglomeration mechanisms in GOTHIC include thermal diffusion, turbulent shear, and gravitational collection and it is assumed that these mechanisms operate independently and that the total agglomeration rate is the sum of the rates for the individual mechanisms. In GOTHIC when a monodisperse field is characterized as uniform the mechanisms that require a size distribution are ignored. The deposition mechanisms in GOTHIC include deposition due to gravitational settling, impaction, thermal and turbulent diffusion, thermophoresis and diffusiophoresis and it is assumed that these mechanisms operate independently and that the total deposition rate is the sum of the rates for the individual mechanisms. The deposition models are applied to each drop field separately.

Turbulent agglomeration and deposition and impaction by thermophoresis and diffusiophoresis were not investigated in this study. These parameters are collected together in Table 1.

Table 1. Aerosol model parameters

Parameter/Model	Value/Flag
Field and injection GSD	1.0
Min. drop Vf	default
Thermal Equilibrium	No
Velocity Equilibrium	No
Entrainment	Yes
Agglomeration	
Interfield Agglomeration	Yes
Intrafield Agglomeration	Yes
Thermal Diffusion	Yes
Turbulent Diffusion	No
Gravitational Collection	Yes
Deposition	
Impaction	Yes
Gravitational Settling	Yes
Turbulent Diffusion	No
Thermophoresis	No
Diffusiophoresis	No

Agglomeration models in GOTHIC are based on the monodisperse agglomeration model described by Hinds (1982). Interfield agglomeration occurs when two drops within a field collide and intrafield agglomeration occurs when drops from separate fields collide. In GOTHIC, when two drops collide and combine, it is assumed that the single resultant drop is in the field that originally held the larger of the two drops (Lane, et al., 2018). GOTHIC integrates agglomeration kernels over a drop size distribution. The agglomeration kernels have the form

$$K_m = A_c(d_a + d_b)u_r(d_a, d_b)\, e_m(d_a, d_b) \tag{13}$$

where $A_c(d_a + d_b)$ is the collection area, $u_r(d_a, d_b)$ is the relative velocity for colliding, and $e_m(d_a, d_b)$ is the capture efficiency, all of which are dependent on the drop diameters d_a, d_b and the agglomeration mechanism.

The agglomeration at each time step for a drop field in a particular location is calculated as the sum of the distinct agglomeration kernels.

Deposition area in GOTHIC is controlled by the volume (or cell) hydraulic diameter, formulated in GOTHIC as

$$A_{w,dep} = \frac{4V}{6D_h} \tag{14}$$

At this stage of work the deposition area is set based on limited PWR assembly dimensions in the open literature. Deposition area in the existing model is considered an approximation based on limited information and the coarse mesh currently in use.

7. ANALYSES

In the current work, a steady state thermal-hydraulic solution is achieved prior to aerosol injection. The same approach was taken for all of the aerosol cases described next. An important note first is on the distinction of size distribution of the injected aerosol from the assumptions of size distribution of the field modeled with GOTHIC. In GOTHIC a monodisperse field is defined as "Uniform" with a GSD=1.0 and a polydisperse field is defined with an initial GSD > 1.0. Polydisperse cases in the current work have 1 or 2 fields defined with an initial GSD=1.5. However, in all cases the aerosol is injected as monodisperse. In select cases where the aerosol field is defined as polydisperse, the injected aerosol will evolve over time to become polydisperse (i.e., the field GSD changes with time). Gravitational collection and size-preferential deposition, emergent from a size distribution, are modeled when the field GSD (tracked by GOTHIC) is greater than 1.0. Monodisperse cases do not include agglomeration by gravitational collection which requires a size distribution. In all cases the aerosol field SMD evolves according to the influence of agglomeration and deposition kernels considered (i.e., models activated according to Table 1). Table 2 summarizes the parameters and mechanisms for all cases in this work.

A set of cases for varied aerosol injection location are designed to evaluate differences in mixing and the estimated time to achieve an approximately uniform concentration throughout the TSC.

The following cases for the size of injected particles and target concentrations were analyzed in this work:

Monodisperse cases: 1 μm AED

Case 1: 1 mg/m^3 initial concentration.

Case 2: 10 mg/m^3 initial concentration.

Case 1b: 1 mg/m^3 initial concentration.

Case 2b: 10 mg/m^3 initial concentration.

Bidisperse cases with two monodisperse fields: 0.5 and 5.0 μm AED

Case 3: 0.5 mg/m^3 initial concentration for both 0.5 and 5.0 μm AED, 1.0 mg/m^3 total.

Case 3b 2.14 mg/m^3 initial concentration for both 0.5 and 5.0 μm AED, 4.28 mg/m^3 total.

Case 3e 5.0 mg/m^3 initial concentration for both 0.5 and 5.0 μm AED, 10.0 mg/m^3 total. Aerosol injected into 2 channels.

Case 3f 5.0 mg/m^3 initial concentration for both 0.5 and 5.0 μm AED, 10.0 mg/m^3 total. Aerosol injected into upper plenum.

Case 3g 5.0 mg/m^3 initial concentration for both 0.5 and 5.0 μm AED, 10.0 mg/m^3 total. Aerosol injected evenly into bottom of all channels.

Polydisperse cases with one and two fields

Case 2c: 10 mg/m^3 initial concentration, GSD=1.5

Case 3c: 0.5 mg/m^3 initial concentration for both 0.5 and 5.0 μm AED, 1.0 mg/m^3 total, GSD=1.5 for the 0.5 + 5.0 μm mixed field

Case 3d: 0.5 mg/m^3 initial concentration for both 0.5 and 5.0 μm AED, 1.0 mg/m^{3}total, GSD=1.5 for two fields with SMD corresponding to 0.5 μm and 5.0 μm AED

Cases 3e, 3f, and 3g are identical except for the aerosol injection locations.

Aerosol parameters for the analyzed cases are summarized in Table 3. The parameters in Table 3 are determined by the injected particle size, density, and target concentration prior to simulation with GOTHIC.

Table 2. Analysis case matrix with aerosol modeling parameters.

	Cases 1, 1b, 2, 2b	Cases 3, 3b, 3e	Case 3f	Case 3g	Cases 2c, 3c	Case 3d
# Injected sizes	1	2	2	2	1	2
# Fields	1	1	1	1	1	2
Injected size distribution	monodisperse (GSD=1.0)	2 monodisperse (GSD=1.0)	2 monodisperse (GSD=1.0)	2 monodisperse (GSD=1.0)	monodisperse (GSD=1.0)	monodisperse (GSD=1.0)
GOTHIC field	monodisperse (GSD=1.0)	monodisperse (GSD=1.0)	monodisperse (GSD=1.0)	monodisperse (GSD=1.0)	polydisperse (GSD=1.5)	polydisperse (GSD=1.5)
Interfield agglomeration (requires 2 or more fields)	NA[1]	NA	NA	NA	NA	✓
Intrafield agglomeration	✓	✓	✓	✓	✓	✓
Agglomeration via thermal diffusion	✓	✓	✓	✓	✓	✓
Agglomeration via gravitational collection (requires GSD > 1.0)	NA	NA	NA	NA	✓	✓
Impaction	✓	✓	✓	✓	✓	✓
Gravitational settling	✓	✓	✓	✓	✓	✓
Injection location	1 channel	2 channels	Upper plenum	Bottom of all channels	1 channel (2c) 2-channels (3c)	2 channels

1. Not applicable for monodisperse field.

Table 3. Aerosol characteristics for the injected size, density, and target concentration.

	Case 1	Case 1b	Case 2	Case 2b, 2c	Case 3, 3c, 3d	Case 3b	Case 3e
AED (µm)	1	1	1	1	0.5, 5.0		
Sauter Mean Diameter[1] (µm)	0.302	0.302	0.302	0.302	0.151, 1.51		
Concentration (mg/m^3)[2]	1	4.38	10	43.8	0.5	2.14	5.0
Mass (mg)[3]	5.78	25.32	57.8	253.21	2.89	12.37	28.9
Volume fraction in cask[4]	9.12×10^{-11}	3.99×10^{-10}	9.12×10^{-10}	3.99×10^{-9}	4.56×10^{-11}	1.95×10^{-10}	4.56×10^{-10}
Injection rate (mg/s)[5]	0.578	2.532	5.78	25.321	0.289	1.237	2.89
Particle count density (#/m^3)	6.33×10^{9}	2.77×10^{10}	6.33×10^{10}	2.77×10^{11}	2.53×10^{10} 2.53×10^{7}	1.08×10^{11} 1.08×10^{8}	2.53×10^{11} 2.53×10^{8}
Particle surface area density (m^2/m^3)	1.81×10^{-3}	7.94×10^{-3}	1.81×10^{-2}	7.94×10^{-2}	1.81×10^{-3} 1.81×10^{-4}	7.75×10^{-3} 7.75×10^{-4}	1.81×10^{-2} 1.81×10^{-3}
Minimum volume fraction[6]	1.44×10^{-14}				1.80×10^{-15}, 1.80×10^{-12}		
Minimum concentration (mg/m^3)	1.58×10^{-4}				1.98×10^{-5}, 1.98×10^{-2}		

1. Sauter mean diameter is equal to the geometric and count median diameter for monodisperse particle size.
2. Bidisperse concentrations, mass, volume fraction, and injection rates are equal for both particle sizes.
3. The cask internal fluid volume is approximately 5.78 m^3 (204.1 ft^3).
4. This is the well mixed uniform distribution volume fraction.
5. Scaled concentrations in cases 1 and 2 assumed a cask average T=200 C. Case 3 scaled concentrations assumed T=210 C.
6. Minimum volume fraction corresponds to a concentration of 1 particle per cm^3.

This page is intentionally left blank.

8. RESULTS AND DISCUSSION

Aerosol behavior is influenced by thermal hydraulic conditions within the cask. A constant decay heat for the initial cask loading power level results in a stabilized natural recirculation mode of decay heat transfer to the cask exterior. This recirculation drives upward flow in 37 fuel tubes each with a local gas flow and velocity. The local gas flow and temperature conditions are determined by the cask decay heat configuration and power level, internal geometry and flow friction, heat transfer resistance to the exterior, and the exterior boundary conditions. This study focused on the initial decay heat solution although decay heat of spent fuel decreases with time and affects changes to the cask internal flow and temperature, resulting in changes to aerosol behavior.

8.1 Thermal Hydraulic Solution

A steady state thermal hydraulic solution for the cask initial loading configuration described in 5.1.2 is achieved prior to aerosol injection. The thermal hydraulic solution is presented before discussing aerosol behavior, which is strongly influenced by the thermal hydraulics. In our model the aerosol energy and transport are coupled to the thermal hydraulics however the influence of aerosol on thermal hydraulics is negligible in the current work with small amounts of injected aerosol mass and energy. The steady state solution is for natural recirculation of He gas internal to the TSC and heat transfer. He gas is heated by fuel assembly decay heat within each fuel tube and cooled by transferring heat to the TSC boundary, resulting in a density gradient that drives natural circulation. During circulation He flows upward through all fuel tubes and circulates through the upper plenum, bypass volume, lower plenum, and then returning to the fuel tubes. The TSC shell exterior is cooled by air passing between the TSC and concrete cask.

Fuel temperature, including peak clad temperature (PCT), and the internal gas temperature and circulation flow rates are sensitive to the decay heat, hydraulic resistance, and heat transfer resistance to the exterior. He temperature and velocity magnitude inside the TSC are shown in Figure 14. He gas flow within the TSC is shown in Figure 15.

The range of He gas velocities in fuel tubes is 2.0-2.5 cm/s. Peak velocities appear in the plena and bypass. Turbulent flow conditions are expected in these regions and will require more evaluation for determining the effects on aerosols within the TSC. GOTHIC has several turbulence models however an evaluation for the selection and use of a turbulence model has not been performed yet. The average channel He mass flow rate is 465 mg/s and the total recirculation flow is 17.21 g/s (61.94 kg/hr). Velocity and mass flow rate distributions apparent in each fuel tube in Figure 14 and Figure 15 are due to interpolation of cell face and cell-center values. The solution for cell-center vertical velocity has a non-slip assumption for velocity at the fuel tube surface.

Comparison of the GOTHIC solution peak vertical velocity in the TSC basket and PCT are compared with higher resolution COBRA-SFS and STAR-CCM+ models of a PWR spent fuel dry storage cask with similar decay power loading configurations and cask boundary conditions (Fort, Michener, Suffield, & Richmond, 2016) in Table 4. Comparison with higher resolution models provides a reasonable check of the GOTHIC solution although differences in the solution are expected due to differences in model element sizes and the particular solution approaches. GOTHIC calculations for the assembly PCT and flow conditions are based on a relatively coarse 1D mesh of the fuel tubes that does not model the fuel pins individually. In our model we have treated each fuel tube assembly individually with an axial power shape, but we have not treated the fuel pins individually. Both COBRA-SFS and STAR-CCM+ models treated each assembly individually with a fuel pin-power distribution (radial peaking factor) and modeled the subchannel fluid dynamics.

The GOTHIC solution compares favorably to high resolution models and demonstrates that our model predicts the natural circulation flow patterns and temperature gradients within the TSC for a particular spent fuel assembly loading configuration and cask boundary conditions.

Table 4. Comparison of GOTHIC PCT and He velocity to COBRA-SFS and STAR-CCM+

	GOTHIC	COBRA-SFS	STAR-CCM+
PCT (°C)	305	302	307
Peak vertical He velocity in fuel tubes (cm/s)	2.5	6.0	3.0

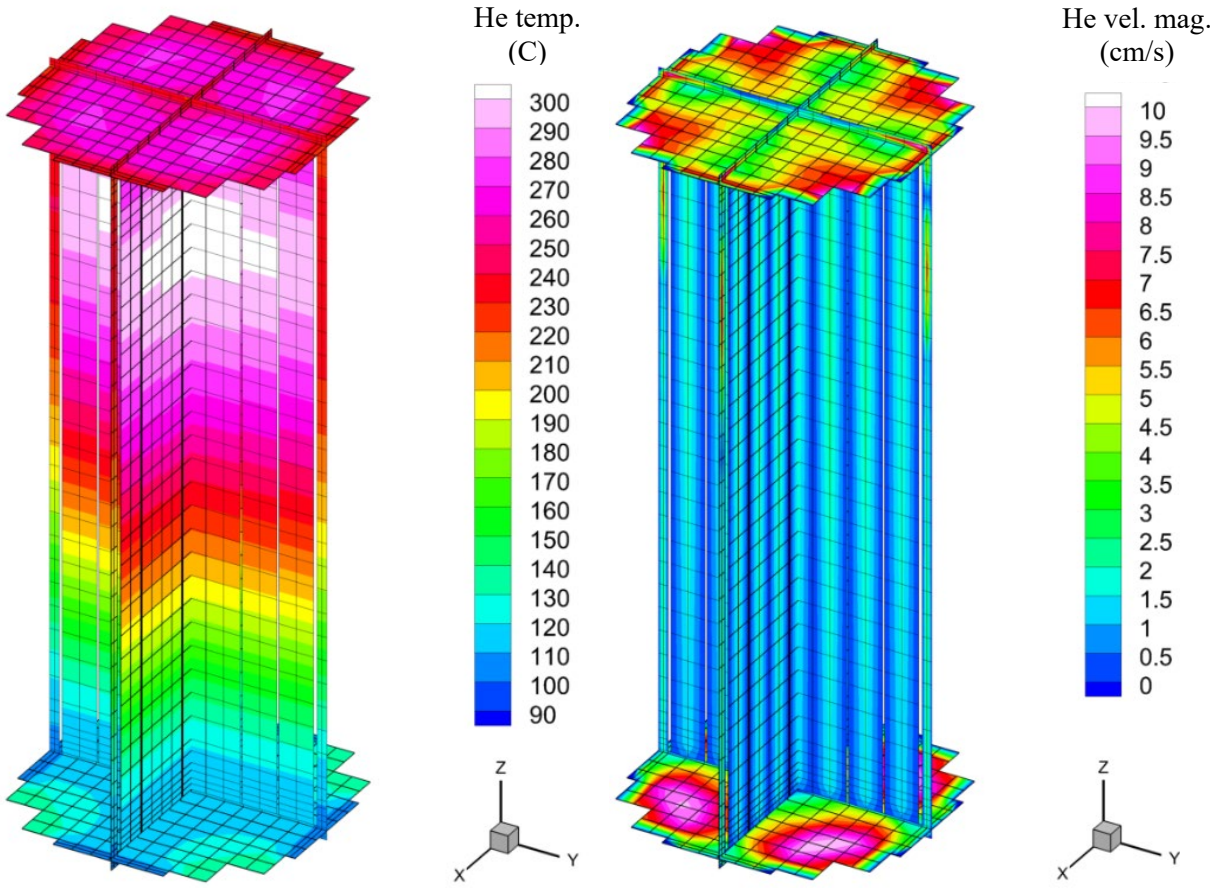

Figure 14. TSC internal He gas temperature (left) and He gas velocity magnitude (right)

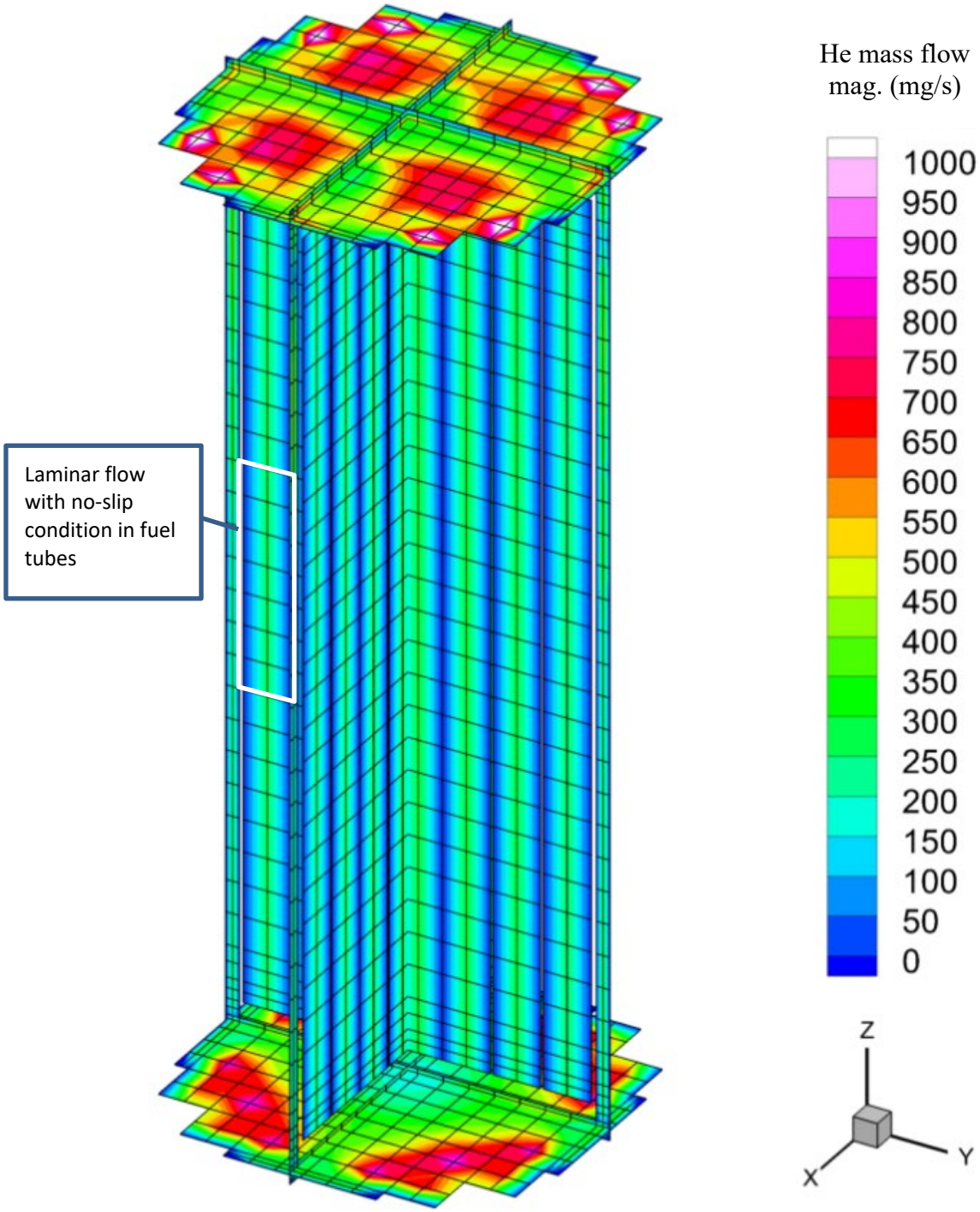

Figure 15. Magnitude of He mass flow rate in TSC.

8.2 Aerosol Settling and Deposition

A uniform mixing of the aerosol was sought to provide a baseline for potential code-to-code comparisons; however, this presents challenges due to the transient solution approach of GOTHIC and because GOTHIC does not provide an option to initialize a simulation with aerosols suspended in a vapor environment. Our approach was to inject the aerosol in one (or two) of the fuel tubes and simulate the following transport and mixing, which are strongly influenced by thermal hydraulic conditions within the TSC. Once the aerosol is injected it mixes during transport through the cask fuel tubes, plena, and bypass region. Gradually the concentration becomes approximately uniform throughout the cask although aerosol mechanics begin to alter the concentration and SMD immediately upon entering.

GOTHIC by default resolves particle count densities down to 1 particle per mL by tracking particles while the particle volume fraction is above a default minimum particle volume fraction α_{min}. The default minimum particle volume fraction is calculated from the particle diameter (Eq. 5) for a count density of 1 particle per cm^3. The smallest diameter should be used to calculate the minimum volume fraction when introducing two or more disparate particle sizes (e.g. 0.5 and 5.0 μm). We found that by not lowering the default minimum volume fraction for the mixed 0.5 + 5.0 μm field that GOTHIC simply did not track the smaller particles once the mixed particle volume fraction dropped below the default and this was apparent in the mass deposition time history where only a fraction of the injected particle mass is seen to have deposited out after 100,000s. Lowering the minimum volume fraction from the default to $1.0x10^{-15}$ improved the calculation and the total deposited mass increased to 95% of the injected mass. In all cases particles were tracked down to a count density of 1 particle per cm^3.

Time step stability was an issue for the polydisperse two-field model. Time step size was reduced by a factor of 4 from 0.06 to 0.015 s. Monodisperse simulations ran smoothly with a time step of 0.06 s, which is just below the CFL limit fixed by maximum flow rate and mesh size. Stability issues originate in the drop-gas interface heat and mass transfer and momentum balance. The temperature equilibrium model was used to ignore temperature differences between particles and vapor in the polydisperse two-field calculation. Particle temperature is set to the gas temperature with this assumption by setting the interface area for heat transfer to a very large value. More investigation is necessary to better understand the time step limitations affecting the solution.

The TSC upper plenum was chosen for a fixed location within the cask for case-to-case comparisons of the aerosol properties. Mixing of the aerosol laden gas streams exiting the fuel tubes into the upper plenum makes this a good location to sample the aerosol properties. Figure 16 provides an overview for concentration in the TSC upper plenum for all cases. Peak concentrations in each case are consistent with the injected mass for each case estimated to result in the respective target STP or scaled concentration indicated in the label for each curve. The peak concentrations are slightly less than the target concentration due to deposition and settling of particles occurring as the aerosol gradually mixes. The early rise and oscillation of concentration is indicative of a higher concentration ensemble circulating in the TSC. After mixing, the concentration decline is gradual initially then followed by accelerating decline. Aerosols remain suspended for longer times in cases with larger initial concentration.

Polydisperse (GSD=1.5) concentrations are marked by dashed lines in Figure 16. Notably, polydisperse concentrations deplete faster. The increased deposition rates of polydisperse fields can be attributed to the larger fraction of larger particles initially present and subsequently produced by agglomeration by gravitational collection. The polydisperse field has a larger fraction of both smaller and larger particles compared with the singular SMD in the monodisperse case.

Aerosol concentrations for the polydisperse 0.5 and 5.0 μm 2-field case are shown in Figure 17 together with the 0.5 and 5.0 μm 1-field polydisperse and monodisperse concentrations for comparison. In the 2-field case two separate polydisperse fields are modeled with initial SMD of 0.5 and 5.0 μm. The concentration for the 0.5 and 5.0 fields are shown separately as dash-dot curves. The mixed concentration is shown as a dashed curve.

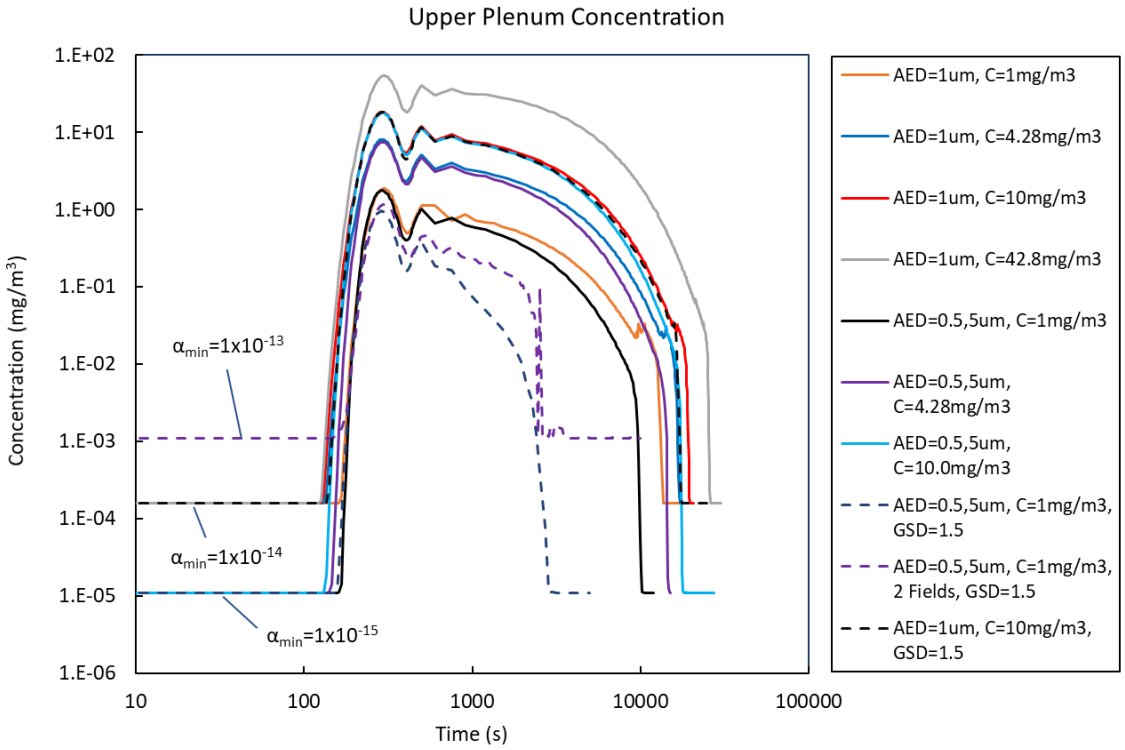

Figure 16. Aerosol concentration in TSC upper plenum.

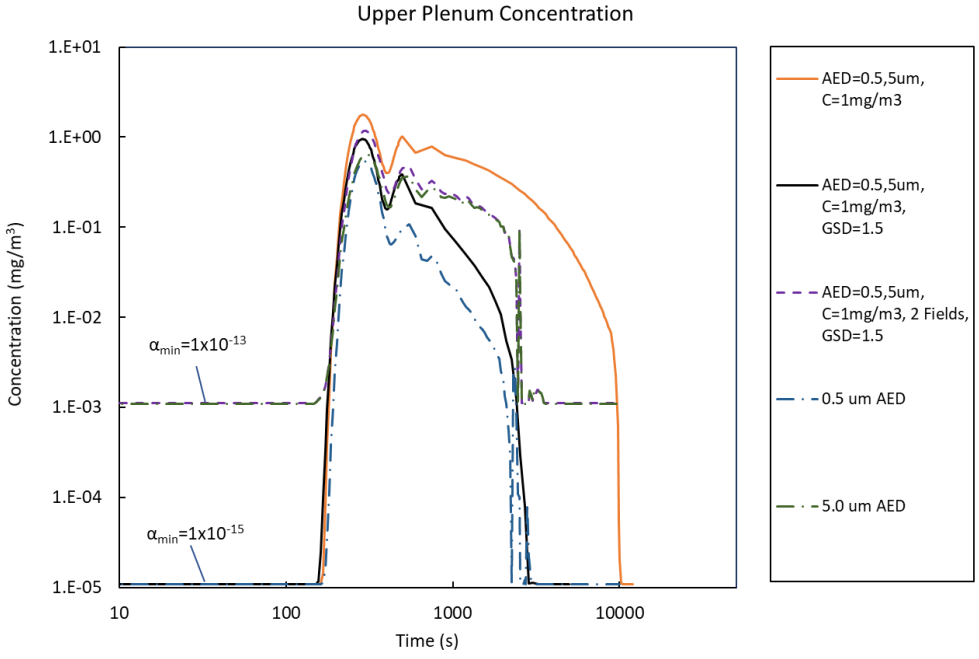

Figure 17. Concentration for 0.5 µm + 5.0 µm cases: 1) one field, GSD=1.0, 2) one field, GSD=1.5, and 3) two fields, GSD=1.5. Concentrations for the 0.5 um, 5.0 µm, and mixed 0.5 + 5.0 µm fields are shown separately.

Aerosol depletion times are shown in Figure 18 and summarized Table 5. Depletion starts immediately following initial injection and ends when the aerosol volume fraction drops below the minimum volume fraction, α_{min}. Depletion time is increased for higher concentrations as evidenced by the trend for monodisperse 1.0 µm cases. While depletion times for the monodisperse mixed 0.5 µm and 5.0 µm cases follow the same trend, the depletion times are less than the 1.0 µm cases with the same concentration. The SMD for monodisperse 0.5 µm + 5.0 µm cases, calculated with Eq. 6, is initially 0.63 µm.

Depletion time was significantly lessened when representing the field as polydisperse. The agglomeration rate for polydisperse fields is expected to be higher due to intrafield thermal agglomeration and gravitational collection, which arise from a size distribution not present in monodisperse fields. The distribution of particle sizes in a polydisperse field results in a distribution of relative velocities and increases collision probabilities. Also, the smaller particles diffuse more readily increasing agglomeration by thermal diffusion and deposition. Although it's clear from the calculations and reasonable that polydisperse fields deplete faster, further study is needed to quantify the mechanisms to determine which mechanisms are driving the results. The longer depletion time for monodisperse fields suggest the use of monodisperse models would provide bounding estimates in some instances for release consequence while polydisperse models provide a best estimate.

Depletion time in the two-field case is ~4 min less than in the one field case. It's possible that interfield agglomeration creates larger particles that settle quicker, increasing deposition rates. Deposition by inertial impaction affects larger particles present in the two-field case. The use of two fields is a more accurate representation for injected sizes that differ by an order of magnitude.

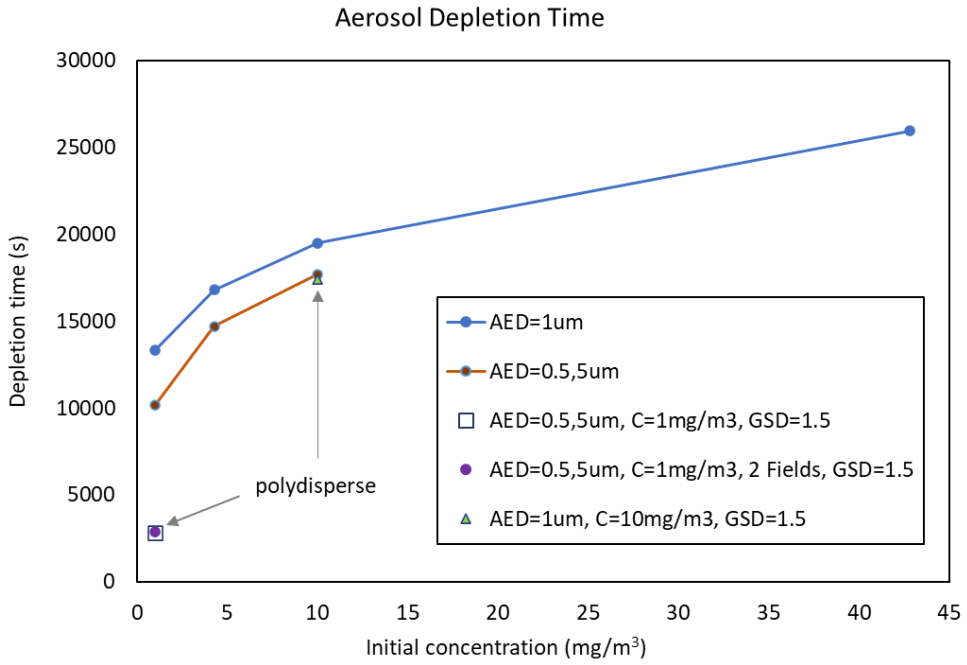

Figure 18. Aerosol depletion times.

Table 5. Aerosol depletion time for all cases sorted shortest to longest.

Case	AED (µm)	Concentration (mg/m^3)	Depletion time (min)
3c	0.5,5; GSD=1.5	1.0	47.5
3d	0.5, 5.0; 2 fields, GSD=1.5	1.0	48.4
3	0.5, 5.0	1.0	172.6
1	1.0	1.0	225.1
3b	0.5, 5.0	4.28	247.6
1b	1.0	4.28	282.6
2c	1.0; GSD=1.5	10.0	290.1
3e	0.5, 5.0	10.0	295.0
2	1.0	10.0	327.6
2b	1.0	42.8	435.2

The deposition rate of aerosols in all volumes was tracked and integrated over time. The total deposited mass fraction versus time is compared for all cases in Figure 19. All monodisperse cases appear similar with notable exceptions being: 1) lower concentrations deposit faster, and 2) the peak deposition fractions vary and do not achieve 100%. Figure 20 provides a closer look at the deposited fraction for each case. It's apparent that lower concentrations which approach 100% deposition faster encounter the minimum cut-off volume fraction for tracking the aerosol. Transient deposition fractions for each field in the 2-field polydisperse 0.5+5.0 um case are shown in Figure 21, and more closely in Figure 22 together with the 0.5 + 5.0 µm 1-field polydisperse and monodisperse cases for comparison.

Calculations of the deposited particle mass for cases with 1 µm particle diameter ranged between 98.1% and 100.5%. The deviation from expected 100% deposition fraction is attributed to approximation of numerical integration. Deposition calculations for the two cases with 0.5 and 5.0 µm particle size injections, showed that a higher concentration (4.28 mg/m3) case had 98.5% deposited mass and the lower concentration case (1 mg/m^3) had 94.9%. The difference in deposition fraction is likely due to the difference in concentration. The higher concentration case will track deposition, which occurs at a higher rate, for a longer period of time before the count density drops below 1 particle mL.

Deposition in all cases exhibit interesting behavior between 100 and 1000s during the period of mixing when concentration in the TSC is not uniform. Before mixing is complete a higher concentration ensemble circulates through the cask in which deposition and agglomeration vary with flow conditions. Deposition is consistently highest in the combined fuel tubes, compared to other locations, where the surface area density is highest.

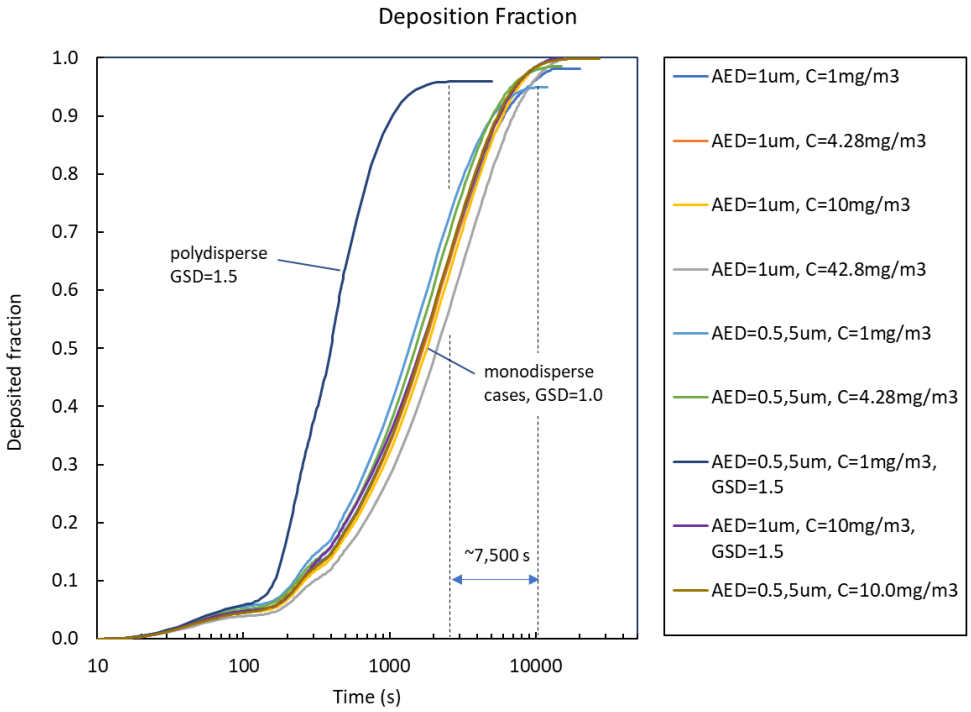

Figure 19. Deposition fractions for the monodisperse baselines and polydisperse case.

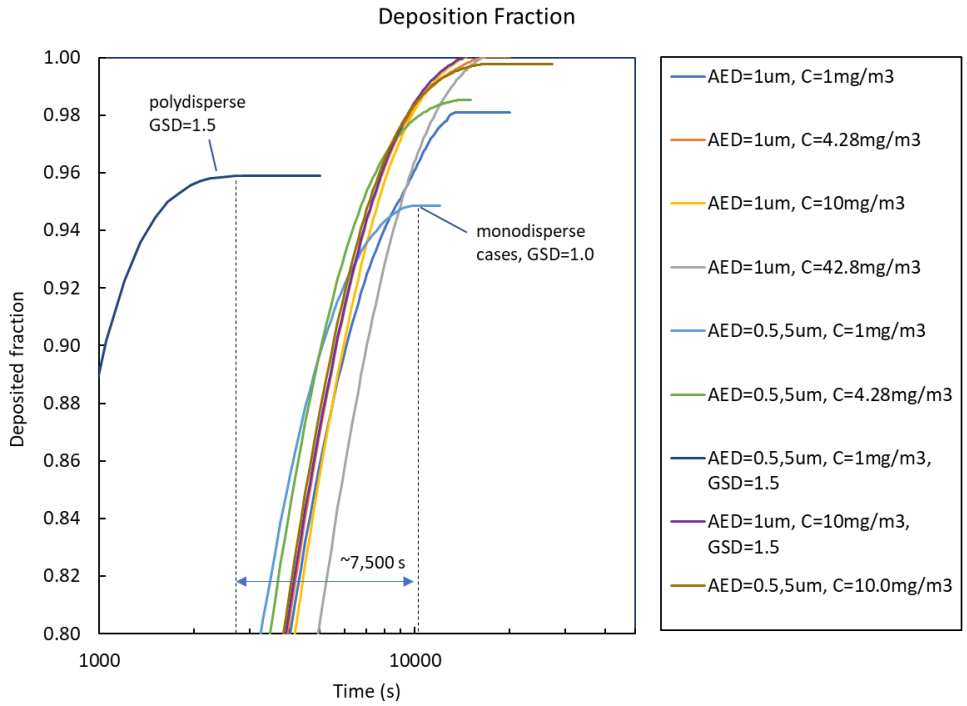

Figure 20. A closer look at the deposition fractions for the monodisperse and polydisperse case.

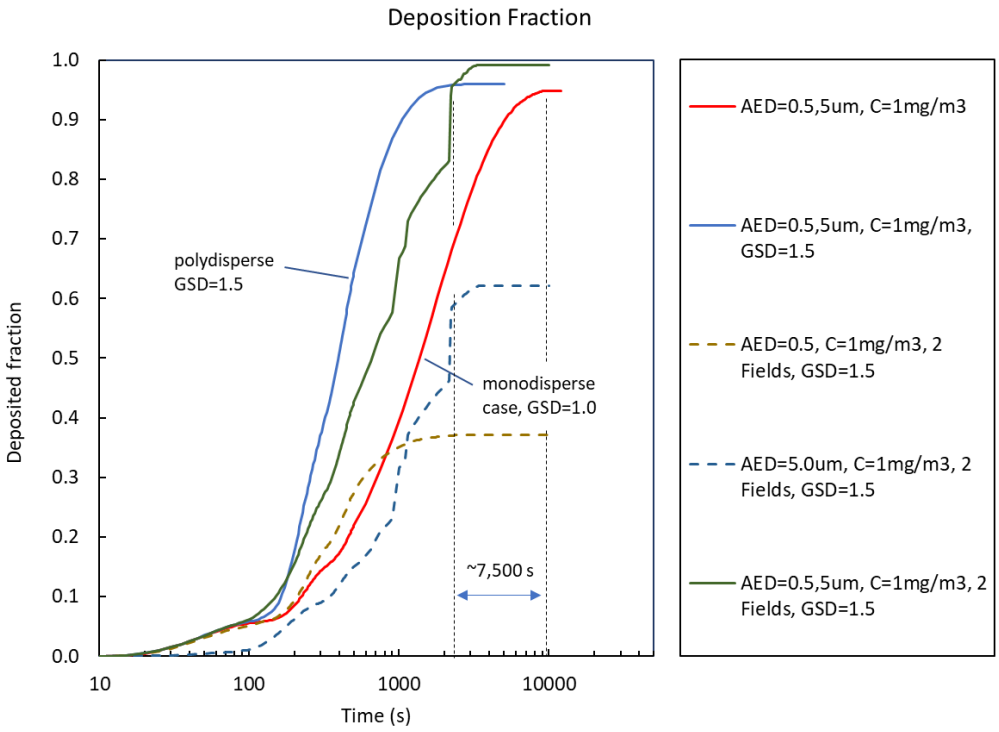

Figure 21. Deposition fractions for the bimodal monodisperse and polydisperse, one field cases and the polydisperse, two field case.

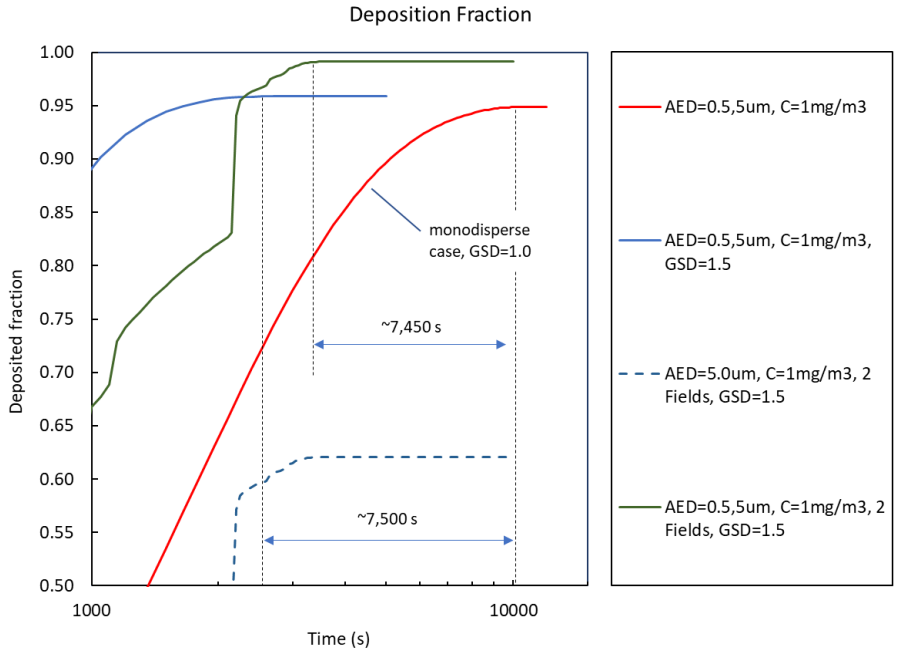

Figure 22. A closer look at deposition fractions for the bimodal monodisperse and polydisperse, one field cases and the polydisperse, two field case.

Table 6 summarizes the end of transient deposition fractions in the upper and lower plena, bypass, and fuel tubes for all cases. The deposition fraction for the lower plenum is consistently around 1-10% except for the 0.5 AED in the 2-field case. Deposition in the lower plenum is likely dominated by settling on the flat horizontal surface at the bottom of the TSC. Deposition in the lower plenum is also a bit higher for case 3c which is a polydisperse case with injection of 0.5 and 5.0 AED particles which suggests that increased deposition in the lower plenum is due to impaction of the larger particles. Deposition in the upper plenum appears to be negligible (<1.0%) except for the 5.0 AED in the 2-field case suggesting that deposition there is most likely caused by inertial impaction, which is expected to be greater for larger particles. Otherwise, in the upper plenum there is little surface area for deposition by diffusion and no horizontal surface to collect settling particles.

Table 6. Deposition fractions for lower and upper plena, fuel tubes, and bypass regions of TSC.

Case	AED (um)	Conc. (mg/m^3)	GSD	Lower plenum	Upper plenum	Fuel tubes	Bypass	Total
1	1	1.0	1.0	3.5%	0.3%	93.5%	0.8%	98.1%
1b	1	4.28	1.0	4.0%	0.3%	94.8%	0.9%	100.0%
2	1	10.0	1.0	5.0%	0.3%	94.1%	1.0%	100.4%
2b	1	42.8	1.0	10.1%	0.7%	88.2%	1.6%	100.5%
2c	1	10.0	1.5	5.3%	0.4%	93.3%	1.5%	100.5%
3	0.5,5.0	1.0	1.0	2.2%	0.3%	91.2%	1.0%	94.9%
3b	0.5,5.0	4.28	1.0	3.3%	0.4%	93.7%	1.1%	98.5%
3c	0.5,5.0	1.0	1.5	7.5%	0.5%	85.0%	2.9%	95.9%
3d (2 fields)	0.5 + 5.0	1.0	1.5	1.4%	17.0%	77.8%	3.0%	99.2%
	0.5	0.5	1.5	0.3%	0.0%	36.1%	0.7%	37.1%
	5.0	0.5	1.5	1.1%	17.0%	41.7%	2.3%	62.1%
3e	0.5,5.0	10.0	1.0	4.6%	0.5%	93.4%	1.2%	99.7%

The SMD and the AED for monodisperse 1.0 µm and 0.5 + 5.0 µm AED cases are shown in Figure 23. Comparing the 1.0 µm cases that have a range of aerosol concentrations (1.0, 4.28, 10.0, and 42.8 mg/m^3), the transient SMD is observed to be progressively larger for each increase to the concentration.

The 1-field 0.5 + 5.0 µm case appears to have the smallest diameter. The initial mixed diameter in the 0.5 + 5.0 µm cases can be estimated with Eq. 6. For d_1=0.5 µm and d_2=5.0 µm and equal concentrations, the resulting diameter is 0.63 µm. This agrees fairly well with the AED for 0.5 + 5.0 µm bidisperse cases shown in Figure 23. AED scales as the SMD times the square root of particle material density (Eq. 9) and provides the diameter of a water drop with the equivalent inertia and settling velocity. The bidisperse 0.5 + 5.0 µm cases appear similar to the monodisperse during most of the transient but does not exhibit the variability that occurs just prior to 100% depletion in the monodisperse cases.

It is apparent that most of the variation in diameter for monodisperse cases occurs later when concentrations are lower and that monodisperse concentrations require longer time to deposit. The prolonged period where the diameter is not changing suggest there is a threshold concentration for

agglomeration. It is possible that agglomeration increases size, while deposition preferentially removes the larger aerosols.

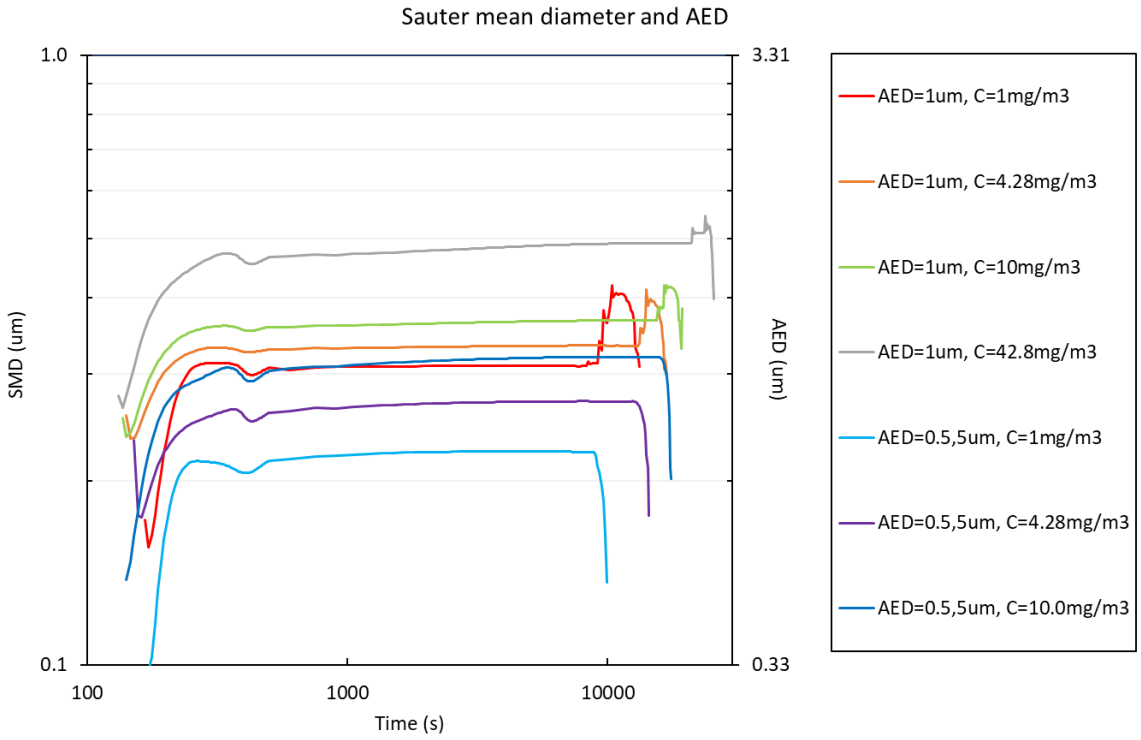

Figure 23. Sauter mean diameter (SMD) and the aerodynamic equivalent diameter (AED) in the cask upper plenum for the 1.0 µm and 0.5 + 5.0 µm monodisperse cases.

SMD and AED for the 1.0 µm polydisperse and 0.5 + 5.0 µm cases are shown in Figure 24. The 1.0 µm polydisperse case appears similar to the monodisperse result shown in Figure 23 although the diameter changes just before depletion appear to occur faster. The 0.5 + 5.0 µm monodisperse shown in Figure 24 is the same case also shown in Figure 23 and is included for comparisons to the polydisperse cases. All 0.5 + 5.0 µm polydisperse cases appear quite different when compared to the monodisperse cases. Deposition occurs much faster and the transient diameter reveals more variability.

A two aerosol field case is compared to the one field case (both polydisperse cases). In this two field case the mixed diameter (curve 1) is much larger than in the one field case (curve 2). This could be caused by agglomeration and faster depletion of the smaller diameter particles. The SMD for each of the separate fields is also shown in Figure 24. The mixed diameter approaches the larger SMD as the transient progresses. SMD for the initial 0.5 µm field, while comparable to the monodisperse 0.5 + 5.0 µm SMD, increases over the transient due to agglomeration of the smaller particles.

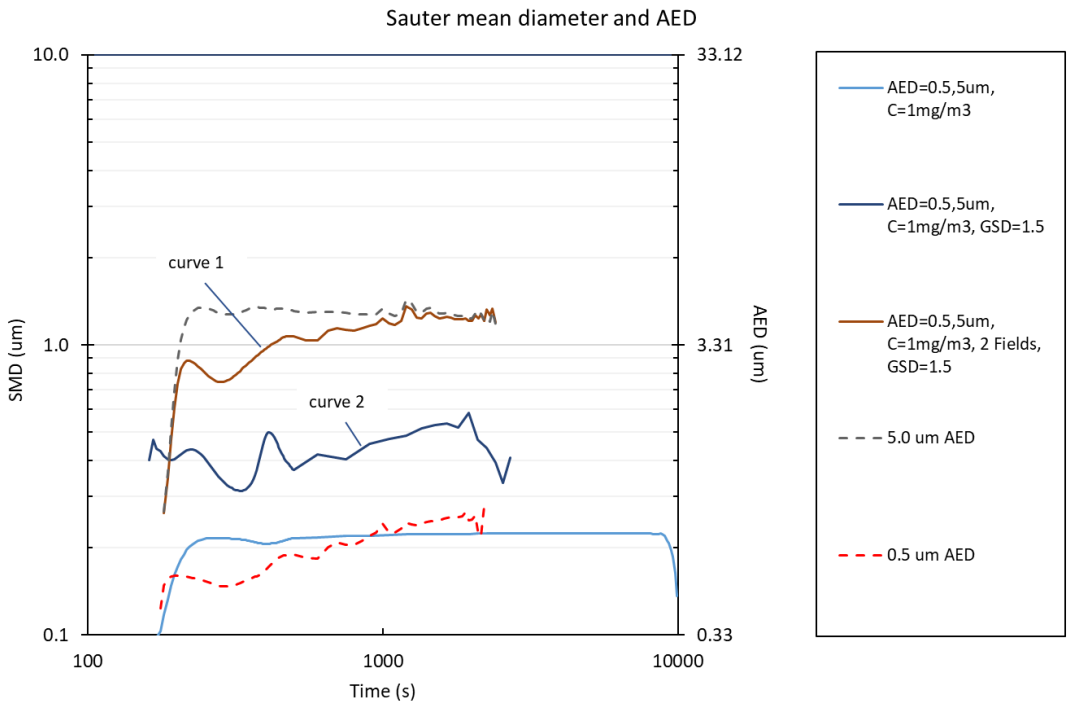

Figure 24: Sauter mean diameter (SMD) and the aerodynamic equivalent diameter (AED) in the cask upper plenum for the 0.5 + 5.0 µm cases.

The GOTHIC drop entrainment model was activated but no entrainment was predicted in any case. The reason for this is unclear but likely due to lack of an entrainment model for dry aerosol. GOTHIC does include entrainment of liquid drops based on hydrodynamics of wavy films and pools of liquids. The correlation for drop entrainment from liquid surfaces depends on liquid film surface, which requires a finite liquid volume fraction, which is not present in our model of a dry cask interior and dry aerosol. Research is necessary to determine what entrainment models are suitable for dry particle uplift and entrainment and compatible with the aerosol modeling approach in GOTHIC.

8.3 Aerosol Mixing

Three aerosol injection schemes have been evaluated to determine the effects on transient distribution of the aerosol concentration and mixing time. It should be noted that a uniform distribution of aerosol concentration within the TSC is not favorable due to the flow patterns and temperature gradients within the TSC. Flow patterns affect aerosol settling and impaction. For example, the gravitational settling rate is higher in channels with lower circulation flow, which imparts upward momentum to the particles. In addition, temperature gradients within the TSC will affect aerosol diffusion rates. A perfectly initialized condition of uniform distribution will evolve to distribute according to the circulation flow patterns.

Mixing time is a useful quantity to facilitate comparisons of the injection schemes. However, the definition of well mixed is subject to the physical conditions previously described, which are not exhaustively analyzed at this time. A quantitative definition of well-mixed is adopted that is based on the standard deviation of concentration in the TSC channels. A standard deviation of 1.0 mg/m^3 is chosen as the threshold value here, below which the aerosol is considered to be well-mixed. The chosen value is 10% of the target concentration (10.0 mg/m^3) and is specific to the conditions in this evaluation. The particular value chosen is less important than the relative differences from each injection scheme.

Aerosol concentration at the bottom of each channel at 500 s for each case is shown Figure 25. The transient channel average concentration for each case is shown in Figure 26. The transient standard deviation of concentration is shown in Figure 27. Mixing times for each injection scheme case are summarized in Table 7.

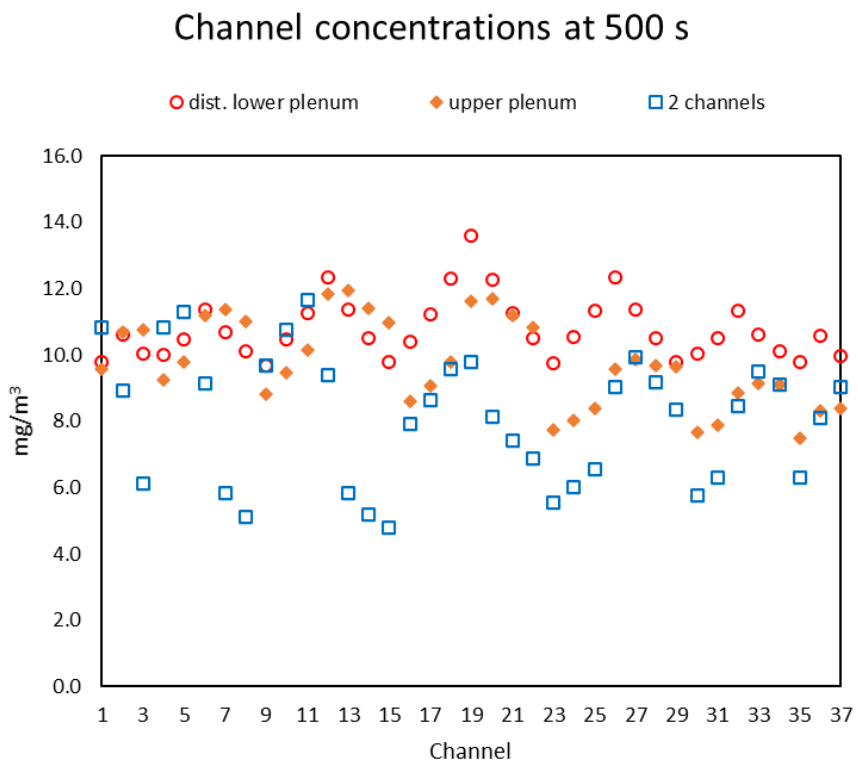

Figure 25. Aerosol concentration in bottom cell of channels at 500 s.

In the 2-channel injection, 0.5 and 5.0 µm sizes were injected into separate channels. Of the three schemes, the 2-channel injection introduces the largest spatial and temporal gradients of concentration and this case had the longest mixing time (900 s). Spatial gradients are introduced by the localized

injection in two channels. A temporal gradient is caused by the 10 s injection duration, which is significantly faster than the He gas circulation period of ~210 s. Localized fast injection results in two high concentration ensembles of particles that circulate in the TSC. GOTHIC predicts the circulation and dispersal of the high concentration ensembles caused by mixing in the plena and bypass region and axial diffusion of particles (i.e., diffusion along the flow stream), as well as the effects of aerosol mechanics.

That the temporal gradient decays in time is evidenced by the decaying fluctuation of concentration at a fixed location as shown in Figure 26. A slower injection time comparable to the circulation period with injection distributed evenly across the channels will minimize spatial and temporal non-uniformity.

Injection in the upper plenum improved the mixing time (735 s). Circulation flow exiting each channel mix in the upper plenum. Monodisperse 0.5 and 5.0 µm particles were injected with vertically upward orientation to deflect on the inner surface of the TSC upper plenum lid. Examining the aerosol concentration in all channels confirmed that 100% of the aerosol is advected by He gas flowing into the bypass region and down to the lower plenum therefore aerosol first enters all channels at the bottom with this injection scheme.

The fastest mixing time (307 s) was achieved with injection distributed evenly across the bottom opening of all channels in the lower plenum. Injection of 0.5 and 5.0 µm particles was spread evenly across the bottom opening of all channels. Examining the aerosol concentration in all channels confirmed that 100% of the injected aerosol was advected by He gas flowing into the bottom of each channel. Figure 26 shows that aerosols enter all channels immediately upon injection, well before the other cases.

The transient effects that appear in the results are subject to thermal hydraulic conditions within the TSC and cannot be nullified. The mixing time can be minimized to a limited extent with more uniform injection schemes. Further evaluation of injection schemes should provide increased value and balance practical considerations of code-to-code comparisons as well as relevance to future aerosol studies.

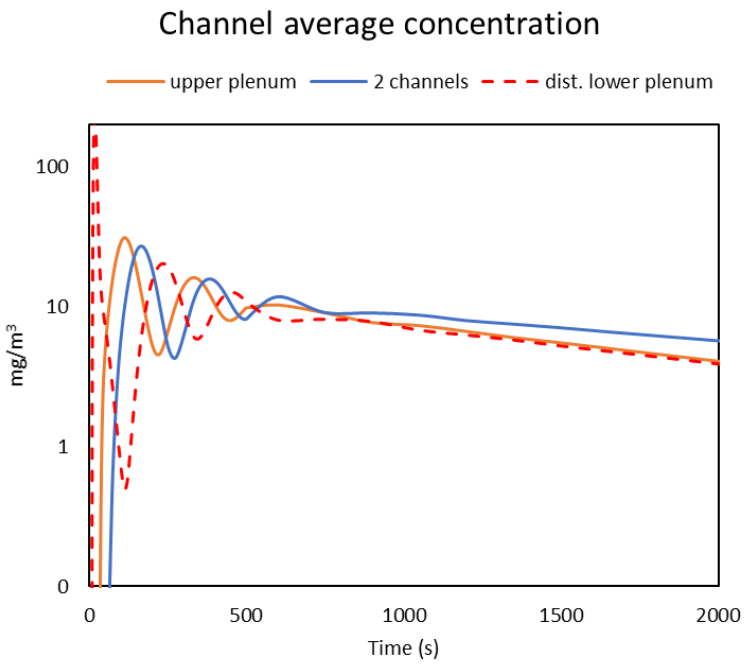

Figure 26. Channel transient average concentration of aerosol in bottom cell of channels.

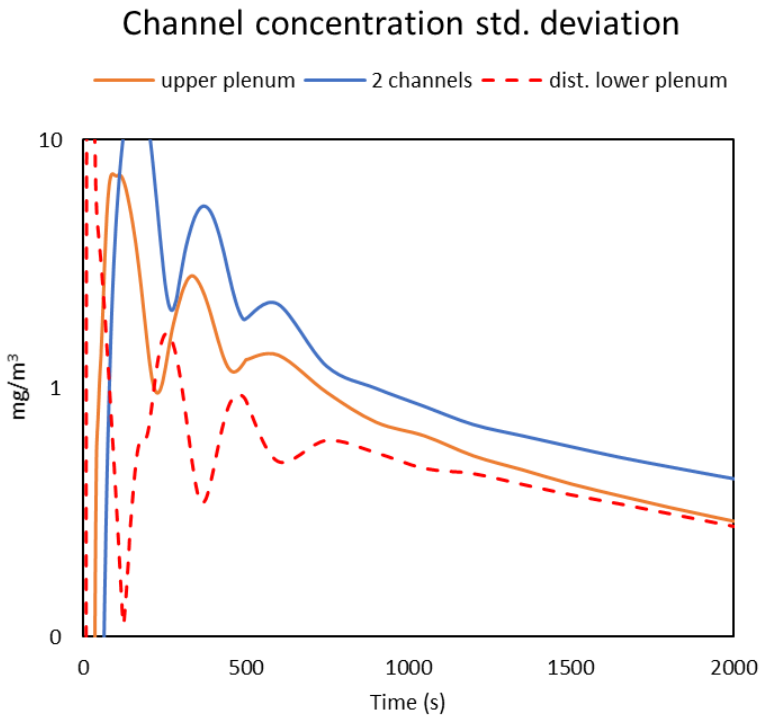

Figure 27. Standard deviation from the average concentration (shown in Figure 23 for t=500s) for aerosol concentrations in the bottom cell of all channels.

Table 7. Mixing times for injection schemes.

Case	Aerosol injection scheme	Time (s) for $\sigma < 1.0$ mg/m^3
3e	2-channel	900 s
3f	Upper plenum	735 s
3g	Distributed evenly into bottom of all channels	307 s

This page is intentionally left blank.

9. CONCLUSIONS

The GOTHIC model being developed to characterize internal conditions within a spent fuel container has been significantly improved from the last version presented in 2019. The model now tracks temperatures and carrier gas flow rates throughout the canister volume. Additionally, suspended particulate movement, agglomeration, and deposition can be tracked. However, several key characteristics of the GOTHIC code came to light in this exercise that impact how the code should be utilized for this effort going forward. For instance, GOTHIC does not offer a convenient method to initialize a simulation with a uniform suspended aerosol field. In order to generate simulations correlating to the baseline cases for comparison to other codes in this effort, a method to initialize a transient with aerosol injection and simulated mixing had to be devised. The influence of non-uniform concentrations and mixing time were characterized for potential aerosol injection schemes and it is believed that this method does provide a consistent basis for comparing calculations. Additionally, it was discovered that GOTHIC struggles with the treatment of particulate populations that deviate from log-normal distributions. When polydisperse populations are allowed in a GOTHIC simulation, the code appears to behave in a more well behaved manner than when only monodisperse or bi-disperse populations are specified. Additionally, minimum particle concentrations and spatial mesh gradients are important parameters in the code and must be set properly in order to obtain accurate tracking of particles down to 1 particle/cm^3 and 100% depletion. Ultimately, the current version of the code provides some insights such as relative predicted depletion times for different initial aerosol conditions and the result that polydisperse populations are predicted to deplete faster than monodisperse or bi-disperse populations. Additionally, the locations within the canister in which preferential deposition is predicted is of interest, with the majority of particulate deposition being predicted for the tubes containing fuel assemblies.

In the first version of the model presented in 2019, the fuel assembly in the central fuel tube of the canister was modeled as a thermal conductor while the fuel in surrounding tubes were treated as heaters. The current version of the code has been updated so that fuel assemblies in all fuel tubes are treated as thermal conductors and the volume (including the plena) has been remeshed. These improvements allow for temperatures and carrier gas flows to be monitored throughout the entire canister volume and allows for more refined comparisons to other codes. A closer inspection of code-to-code comparisons of the thermal hydraulic solution PCT and circulation velocity are favorable with minor differences to be expected based on variances in model resolution and particular approaches. The improved GOTHIC solution demonstrates that our model predicts the natural circulation flow patterns and temperature gradients within the TSC for a particular spent fuel assembly loading configuration and cask boundary conditions. Predictive capability of the TSC internal thermal hydraulics is critically informative to evaluations of aerosol phenomena within the TSC relevant to breach consequence studies. A major advantage of this model is the capability to simulate the complex environment with a relatively low computational cost to provide a practical tool for parametric studies of aerosol transport and depletion while integrating the relevant physics.

The current model is now capable of tracking temperatures, flow rates, and suspended particle behavior throughout the canister, but several parameters remain to be studied to provide further confidence that 1) the numerical performance of the model is optimal and that 2) true heat and mass transport physics are being represented. Currently, several issues are identified for further investigation to provide this confidence as outlined below.

The aerosol deposition area is an important parameter that affects where the aerosol deposits in addition to the flow, temperature, and aerosol properties. GOTHIC calculates the aerosol deposition area from the volume or cell hydraulic diameter, which is also an important parameter for friction drag and heat transfer in GOTHIC. Further work should continue to refine the assembly geometry and determine the optimal hydraulic diameter that provides accurate friction drag as well as wettable surface area for deposition. Also, additional investigation is necessary to quantify the deposition behavior and local accumulation at various locations within the cask.

Further investigation of the extent to which deposition and agglomeration mechanisms are causing the observed results is warranted. GOTHIC integrates the aerosol agglomeration kernels internally, but a method is not yet established to report the agglomeration rate and parse it for the different mechanisms, making it difficult to assess what mechanisms are driving the results. The total deposition rate at every location is a convenient output from GOTHIC but a method to parse that into the different deposition mechanisms is also needed.

The drop entrainment models in GOTHIC are based on hydrodynamics of wavy films and pools of liquids and do not apply to dry aerosols. The correlation for drop entrainment from liquid surfaces requires a finite liquid volume fraction, which is not present in our model of a dry cask interior and dry aerosol field. Research is necessary to determine what entrainment models are suitable for dry particle uplift and entrainment and compatible with the aerosol modeling approach in GOTHIC.

Further investigation into particle settling velocities is needed. The drop-gas momentum balance governs the particle convection and settling relative to the gas flow. This relationship needs to be further explored through a parametric study to elucidate the emergent behaviors from the complex interplay of competing physics modeled in GOTHIC.

Further work is needed to characterize the sensitivity of results to mesh and time step refinements. The TSC internal geometry is challenging to model for a couple reasons. The first is the intricate shapes that describe a fuel assembly with pins, spacer grids, intermediate flow mixers, and nozzles. Second is the relative height of the TSC upper and lower plenum compared with length of the fuel tubes. The plena heights are a factor of 50 times smaller than fuel tubes lengths and cell sizes in the current model mesh are designed to smoothly transition from 1.5” to 12” based on a coarse mesh treatment in the fuel tube region. A finer mesh in the fuel tubes will refine the calculations certainly, but with an increased computational expense.

An investigation of the impact of laminar flow assumptions in neglecting turbulence effects on agglomeration and deposition in upper plenum is desired. The assembly friction drag equation is based on laminar flow conditions and our calculations currently do not use any of the available GOTHIC turbulence models.

Finally, combining the GOTHIC cask model with a higher fidelity computational fluid dynamics model for an assembly in a fuel tube for refined simulation of aerosol transport and deposition on an assembly will provide a great deal of insight into total aerosol behavior in the fuel tubes. This could be achieved through a coordinated collaborative effort to combine the strengths of the current GOTHIC model with the model developed by Fort, Michener, Suffield, & Richmond (2016).

10. REFERENCES

Casella, A. M., Loyalka, S. K., & Hanson, B. D. (2014). Modeling of Particulate Behavior in Pinhole Breaches. *Nuclear Technology, 186*, 99-114. Retrieved from http://dx.doi.org/10.13182/NT13-55

Durbin, S., Lindgren, E., & Pulido, R. (2018). *Measurement of Particulate Retention in Microchannel Flows.* SAND2018-10522-R: Sandia National Laboratories.

Fort, J., Michener, T., Suffield, S., & Richmond, D. (2016). *Thermal Modeling of a Loaded Magnastor Storage System at Catawba Nuclear Station.* Pacific Northwest National Laboratory, PNNL-25871 Rev. 0. U.S. Department of Energy, Used Fuel Disposition Campaign.

GOTHIC. (2018). *Thermal Hydraulic Analysis Package, Technical Manual.*

Heintzenberg, J. (1994). Properties of the Log-Normal Particle Size. *Aerosol Science and Technology, 21*(1), pp. 46-48. doi:10.1080/02786829408959695

Hinds, W. (1982). *Aerosol Technology, Properties, Behavior and Measurement of Airborne Particles.* New York: John Wiley and Sons.

Lane, J., George, T., Claybrook, S., Zankowski, J., Penley, J., & Skelton, P. (2018). *GOTHIC Thermal Hydraulic Analysis Package, Version 8.3(QA) User Manual.* Palo Alto, CA: EPRI.

Lanza, M. S., Azuma, M., Carstens, N., & Casella, A. (2020). *Summary of Progress: Modeling Compressible Flow in Microchannels.* Pacific Northwest National Laboratory Report, PNNL-30239.

Lanza, M., Casella, A., Elsawi, M., Carstens, N., & Springfels, D. (2019). *Thermal Hydraulic Modeling of a Dry Cask and Microchannel.* Pacific Northwest National Laboratory Report, PNNL-29225.

Mitrakos, D., Chatzidakis, S., Hinis, E., Herranz, L., Parozzi, F., & Housiadas, C. (2008). A Simple Mechanistic Model for Particle Penetration and Plugging in Tubes and Cracks. *Nuclear Enginnering and Design, 238*(12), 3370-3378.

NAC International. (2011). *FSAR - Non-Proprietary - MAGNASTOR "Final Safety Analysis Report".* Norcrosse, Georgi: NAC, Rev. 1.

Todreas, N., & Kazimi, M. (2012). *Nuclear Systems Vol. 1* (2 ed.). CRC Press.